Channel coupling and nonorthogonality in elastic and transfer processes*

S. R. Cotanch and C. M. Vincent
Department of Physics, University of Pittsburgh, Pittsburgh, Pennsylvania 15260
(Received 1 March 1976)

The direct reaction $A(a,b)B$ is described by exactly solving the Schrödinger equation for a few-body Hamiltonian within a restricted model space. The model space allows for coupling to rearrangement channels by including basis vectors classified according to different mass partitions. The nonorthogonality of basis vectors that correspond to different mass partitions is investigated in detail. A surface approximation is developed to understand the magnitudes of multistep amplitudes produced by channel coupling to rearranged partitions. The surface approximation uses a separable Green's function approximation to the multistep series, and gives a convenient closed-form expression. Finite-range coupled-channels calculations are presented for the reactions (d,d), (d,p), and (p,p) on oxygen and zirconium targets, and for $(^{16}O,^{16}O)$, $(^{16}O,^{12}C)$, and $(^{12}C,^{12}C)$ on silicon and sulfur targets. To assess higher-order effects, these results are consistently compared with lowest-order results using folded distorting potentials. The calculations indicate that the effects of nonorthogonality are small for these reactions, but the light-ion reactions showed much larger effects. Theoretical explanations of the behavior of nonorthogonality and channel-coupling effects are given, and lead to criteria for predicting when such effects may be important. Channel-coupling effects are expected to be important whenever the distorted-wave Born-approximation transfer amplitude is unusually sensitive to the intermediate channel optical potential. Nonorthogonality effects are roughly proportional to channel-coupling effects, but are much smaller than coupling effects except when a small mass is transferred between two large masses.

[NUCLEAR REACTIONS $^{16}O(d,d)$, $^{16}O(d,p)$, $E=10.49$, 14.8, 20 MeV, $^{17}O(p,p)$, $E=10.98$ MeV, $^{90}Zr(d,d)$, $^{90}Zr(d,p)$, $E=12$ MeV, $^{28}Si(^{16}O,^{16}O)$, $^{28}Si(^{16}O,^{12}C)$, $E=42$, 48 MeV, $^{32}S(^{12}C,^{12}C)$, $E=41.71$ MeV; calculated $\sigma(\theta)$. Folded-potential DWBA plus multistep contribution of rearranged intermediate channels, corrected for nonorthogonality. Surface approximation with separable Green's function.]

I. INTRODUCTION

The distorted-wave Born approximation (DWBA)[1-5] has provided a convenient framework for analyzing direct nuclear reactions and, with several lowest-order refinements, has satisfactorily explained many experimental observations. However, in the last few years improved experimental techniques have enabled measurements which have established that the basic one-step mechanism of the DWBA is inadequate[6-10] to represent certain reactions. These reactions are nevertheless believed to be direct because the cross sections depend smoothly on energy, and can be described in terms of only a few degrees of freedom. This accumulation of evidence has made clear that an improved reaction theory is needed to include higher-order corrections. A 1964 publication by Penny and Satchler[11] describes a procedure [now referred to as the coupled-channels Born approximation (CCBA)] for including excitations of the target and residual nuclei in transfer reactions. In subsequent applications and developments[12-16] of this method large multistep corrections occurred for reactions involving collective nuclei. In CCBA only inelastic channels are included as intermediate states.

In this paper we are concerned with intermediate states of a different type, namely those involving rearrangement of the particles into different mass partitions. As discussed in previous works[17-29] on this subject, the extension to intermediate rearrangement states introduces new difficulties. One major difficulty in including different partitions is that rearrangement always involves the use of a different free Hamiltonian for each partition. Consequently, the free states in different partitions of the system are not orthogonal. In formal reaction theory, this difficulty is avoided by introducing a different interaction for each partition, with the result that the familiar integral expressions for the amplitude can be derived. However, if one wishes to extend coupled-channels ideas to include intermediate rearrangement, one is forced to contend with the nonorthogonality of the basis states. This is the concern of the present work regarding nonorthogonality.

In principle, a description of a direct reaction should include effects of the many-body nature of the system, and yet avoid calculating compound-nucleus aspects of the dynamics. Therefore, we shall assume that the system can be represented

by a few-body model, with complex interactions that allow for the loss of flux into neglected channels and the effects of energy averaging over compound-nucleus fine structure. For example, a four-body model permits a description of a process in which two particles are transferred sequentially, as in the (p,d,t) contribution to the (p,t) reaction. However, for simplicity we restrict the discussion to reactions such as (d,p) and $(^{16}O,^{12}C)$, in which only one particle (or cluster) is transferred, although it may be exchanged several times. A three-body model suffices to describe these processes.

Within the three-body model, several different approaches are still possible. One may attempt to solve the model exactly by Faddeev techniques.[30] However, the Faddeev approach is more appropriate for mathematical proofs than for practical calculations. Furthermore, if separable potentials are used with the Faddeev technique, it is difficult to maintain contact with the extensive phenomenology of optical potentials, which is based on local potential forms.

Because the DWBA has been so successful, it seems more natural to use a technique which gives the DWBA result in first approximations. One such technique, which is not subject to the inconveniences of the Faddeev method, is to expand the complete Green's function in powers of the residual interaction appropriate to a selected partition. Each term of the expansion may then be truncated by retaining only a finite set of bound states of each of the two fragments in the intermediate partition. Kunz[31] has shown that it is possible to devise such a procedure which is equivalent to solving a certain set of coupled-reaction-channel (CRC) equations, and that in this approach no corrections for nonorthogonality of the channel wave functions are required. This approach will be referred to as the unsymmetric interaction coupling (UIC) method. Other, more formal, methods[32-36] also exist which gave DWBA in lowest order and do not require nonorthogonality corrections.

The present work, which also gives the DWBA result as a leading term, uses an alternative method called the model-space (MS) method. We adopt the same point of view as Austern,[19] Ohmura *et al.*,[37] and Udagawa, Wolter, and Coker.[24] Instead of truncating the intermediate states in the terms of a series, we truncate the three-body Hilbert space $\mathcal{L}$ to a definite model space $\mathcal{L}_M$, and then *exactly diagonalize the Hamiltonian within this subspace*. This procedure is perhaps as consistent as it is possible to be, without exactly solving the three-body problem. In the MS method, the nonorthogonality of the basis requires inclusion in the coupled equations of new terms, which are unlike any terms in the familiar coupled equations for inelastic scattering.

It is an open question whether the UIC method or the MS method gives a better approximation to the exact solution of the three-body model, or indeed to the direct-reaction amplitude for the many-body system. This question cannot be decided within the limited scope of the present investigation. However, we shall show by explicit calculation that the nonorthogonality effects are small, at least in certain cases. Where nonorthogonality effects are negligible, the differences between the UIC method and the MS are inconsequential, and can be disregarded in practice.

In different (but strictly equivalent) formulations of the MS, the nonorthogonality effects enter in different ways. In the equations of Ohmura *et al.*, nonorthogonality introduces off-diagonal corrections to the energy and the kinetic energy, as well as corrections to the optical-potential terms. On the other hand, in the work of Udagawa *et al.*, nonorthogonality appears only in the interaction terms. We have performed all our calculations in the Ohmura *et al.* formulation. However, the nonorthogonality effects are easiest to interpret in an extension of the Udagawa *et al.* formulation. This formulation permits all nonorthogonality effects to be related to a single purely geometric quantity—the overlap kernel N that describes the extent to which the basis is nonorthogonal.

Sections II and III describe the mathematical formulation of the MS method and the details of the calculation for reactions involving only s-wave bound states. Section IV describes numerical studies of the effects of nonorthogonality and channel coupling on transfer reactions and elastic scattering. The remainder of the paper describes efforts to understand the magnitude of these effects and their dependence on parameters. We regard this as the main new content of the paper. Section V explains why the nonorthogonality effects are small in the important partial waves, so that the effects of channel coupling can meaningfully be studied without including nonorthogonality corrections. Section VI develops a surface approximation (SA),[38] by which the multistep amplitude is reduced to ordinary DWBA amplitudes. This simplification gives insight into the channel-coupling effects. Finally, Sec. VII develops the consequences of the SA for the (d,p) and $(^{16}O,^{12}C)$ reactions, and the elastic scatterings in each channel. Rules for predicting the dependence of multistep effects on reaction parameters emerge from this study.

The main conclusions are summarized in Sec.

VIII while a mathematical study of the overlap kernel N is relegated to the Appendix.

II. FORMULATIONS OF THE MODEL-SPACE METHOD

In this section the coupled equations of the Ohmura *et al.*[37] formulation of the model-space (MS) method are derived. This formulation is then shown to be equivalent to the two others which are also derived: that of Udagawa *et al.*,[24] and a new formulation which is based on the Ohmura *et al.* approach. The MS equations will be the basis of actual numerical calculation, while the other two formulations will be used for theoretical interpretation of the results. The discussion is restricted to coupling between two different mass partitions, with one channel per partition. However, the results can be generalized to several partitions, each having several channels.

We consider the rearrangement reaction $A(a,b)B$ in which a cluster x is transferred:

$$(b+x)+A \rightarrow b+(x+A).$$

We assume the process can be described in terms of three distinct, inert particles b, x, and A. The coordinate vectors for this three-body system are defined in Fig. 1. Any two of the five vectors

$$\vec{r}_\alpha,\ \vec{r}_{bx},\ \vec{r}_\beta,\ \vec{r}_{Ax},\ \vec{r}_{Ab}$$

may be selected for use as independent coordinates to describe the system. In the center-of-mass frame, the three-body Hamiltonian is

$$H = T_{bx}+T_{Aa}+V_{bx}+V_{Ab}+V_{Ax} \tag{2.1}$$

$$= T_{Ax}+T_{Bb}+V_{bx}+V_{Ab}+V_{Ax}, \tag{2.2}$$

where T_{ij} and V_{ij} are, respectively, the relative kinetic energy and potential energy of particles i and j. We are interested in two specific mass partitions α and β which represent the incident, $a+A$, and exit, $b+B$, arrangements, respectively. In conformity with these partitions the Hamiltonian can be written as

$$H = H_\alpha + T_\alpha + U_\alpha + \hat{V}_\alpha \quad \text{(Prior)} \tag{2.3}$$

$$= H_\beta + T_\beta + U_\beta + \hat{V}_\beta, \quad \text{(Post)} \tag{2.4}$$

corresponding to the post and prior representations. In Eqs. (2.3) and (2.4) the arbitrary distorting potentials U_α, and U_β have been introduced for convenience. The particular form of these interactions is at our disposal since they are also included in the residual interactions $\hat{V}_\alpha$ and $\hat{V}_\beta$:

$$\hat{V}_\alpha = V_{Ab}+V_{Ax}-U_\alpha \quad \text{(Prior)}, \tag{2.5}$$

$$\hat{V}_\beta = V_{Ab}+V_{bx}-U_\beta \quad \text{(Post)}. \tag{2.6}$$

The operators H_α and H_β are the internal Hamiltonians of $a=b+x$ and $B=A+x$:

$$H_\alpha = T_{bx}+V_{bx}, \tag{2.7}$$

$$H_\beta = T_{Ax}+V_{Ax}. \tag{2.8}$$

We introduce the bound-state wave functions ϕ_α and ϕ_β, normalized to unity, which are eigenfunctions of these operators, corresponding to binding energies ϵ_α and ϵ_β, respectively:

$$H_\alpha \phi_\alpha(\vec{r}_{bx}) = -\epsilon_\alpha \phi_\alpha(\vec{r}_{bx}), \tag{2.9}$$

$$H_\beta \phi_\beta(\vec{r}_{Ax}) = -\epsilon_\beta \phi_\beta(\vec{r}_{Ax}). \tag{2.10}$$

The essential idea of the MS method is to diagonalize H within a proper subspace $\mathcal{L}_M$ of the full three-body Hilbert space $\mathcal{L}$. The space $\mathcal{L}$ consists of all square-integrable functions of two independent relative coordinate vectors of the three-body model. The scalar product of two functions f and g in $\mathcal{L}$ is defined by

$$\langle f|g\rangle \equiv \int d\vec{r}_\alpha d\vec{r}_{bx} f^* g$$

$$= \int d\vec{r}_\beta d\vec{r}_{Ax} f^* g. \tag{2.11}$$

The model space $\mathcal{L}_M$ is spanned by the set of vectors $\{\Phi_{\alpha\vec{r}}, \Phi_{\beta\vec{r}}\}$ defined by

$$\Phi_{\alpha\vec{r}} = \delta(\vec{r}-\vec{r}_\alpha)\phi_\alpha(\vec{r}_{bx}),$$
$$\Phi_{\beta\vec{r}} = \delta(\vec{r}-\vec{r}_\beta)\phi_\beta(\vec{r}_{Ax}), \tag{2.12}$$

where the ϕ_γ ($\gamma=\alpha,\beta$) are the bound-state functions defined by Eqs. (2.9) and (2.10). From Eqs. (2.11) and (2.12) the scalar product of two basis vectors belonging to different partitions α and β is[39]

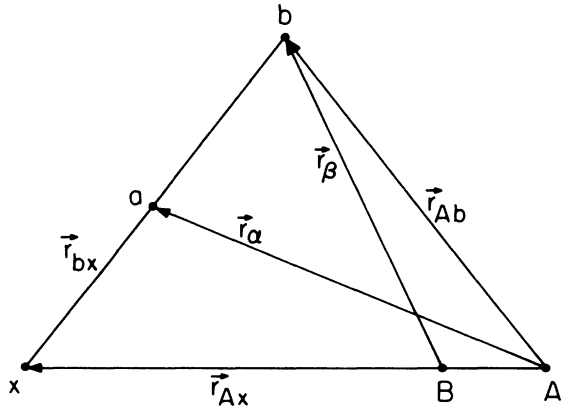

FIG. 1. Coordinates for the reaction $A(a,b)B$ in which a cluster x is transferred. Only two of the five coordinate vectors are independent.

$$N(\vec{r},\vec{r}') \equiv \langle \Phi_{\alpha\vec{r}} | \Phi_{\beta\vec{r}'} \rangle = \int d\vec{r}_\alpha d\vec{r}_{bx}\, \delta(\vec{r}-\vec{r}_\alpha)\phi_\alpha(\vec{r}_{bx})\delta(\vec{r}'-\vec{r}_\beta)\phi_\beta(\vec{r}_{Ax})$$

$$= J \int d\vec{r}_\alpha d\vec{r}_\beta \delta(\vec{r}-\vec{r}_\alpha)\delta(\vec{r}'-\vec{r}_\beta)\phi_\alpha(\vec{r}_{bx})\phi_\beta(\vec{r}_{Ax}) = J\,\phi_\alpha(\vec{r}_{bx})\phi_\beta(\vec{r}_{Ax}), \tag{2.13}$$

with

$$\vec{r}_{bx} = J^{1/3}\left(\frac{A}{B}\vec{r}-\vec{r}'\right), \quad \vec{r}_{Ax} = J^{1/3}\left(\vec{r}-\frac{b}{a}\vec{r}'\right). \tag{2.14}$$

In these equations, J is the Jacobian of the transformation from the coordinates $\vec{r}_\alpha$ and $\vec{r}_{bx}$ to the coordinates $\vec{r}_\alpha$ and $\vec{r}_\beta$. This quantity, which will be of interest in the discussion of nonorthogonality effects, depends only on the masses a, x, and A of the three particles involved:

$$J \equiv \left[\frac{a(A+x)}{x(A+a)}\right]^3. \tag{2.15}$$

Although the vectors (2.12) are not orthogonal, as indicated by Eq. (2.13), they are nevertheless linearly independent. The Appendix contains further discussion of this point. Here we need only remark that the *overlap kernel* N defined by (2.13) vanishes for large r and r', because the bound states are localized. Therefore the vectors (2.12) are at least asymptotically orthogonal.

The MS approach assumes that the model space $\mathcal{L}_M$ includes the important parts of the full space $\mathcal{L}$. The exact three-body wave function Ψ is approximated by the model wave function Ψ_M which is expanded in terms of the basis states $\Phi_{\gamma\vec{r}}$:

$$\Psi_M = \sum_{\gamma=\alpha,\beta} \int d\vec{r}\, \chi_\gamma(\vec{r})\Phi_{\gamma\vec{r}}. \tag{2.16}$$

The subscript $\vec{r}$ on $\Phi_{\gamma\vec{r}}$ should be regarded as a continuous label and not as a variable. The unknown functions $\chi_\gamma(\vec{r})$ are the coefficients of the expansion and are not vectors in the model space $\mathcal{L}_M$. By combining Eqs. (2.12) and (2.16) we obtain the more familiar expression

$$\Psi_M = \chi_\alpha(\vec{r}_\alpha)\phi_\alpha(\vec{r}_{bx}) + \chi_\beta(\vec{r}_\beta)\phi_\beta(\vec{r}_{Ax}). \tag{2.17}$$

To determine the functions χ_γ we diagonalize H within the model space by projecting on to the basis vectors, as follows:

$$\langle \Phi_{\alpha\vec{r}_\alpha} | H - E | \Psi_M \rangle = 0, \tag{2.18}$$

$$\langle \Phi_{\beta\vec{r}_\beta} | H - E | \Psi_M \rangle = 0. \tag{2.19}$$

Here E is the total energy in the center-of-mass frame. This procedure yields two coupled integro-differential equations

$$D_\alpha(E_\alpha)\chi_\alpha(\vec{r}_\alpha) = -\int K_{\alpha\beta}(\vec{r}_\alpha,\vec{r}_\beta)\chi_\beta(\vec{r}_\beta)d\vec{r}_\beta, \tag{2.20}$$

$$D_\beta(E_\beta)\chi_\beta(\vec{r}_\beta) = -\int K_{\beta\alpha}(\vec{r}_\alpha,\vec{r}_\beta)\chi_\alpha(\vec{r}_\alpha)d\vec{r}_\alpha. \tag{2.21}$$

These equations represent the Ohmura *et al.* formulation of the MS method. The differential operators $D_\gamma(E_\gamma)$ are defined by

$$D_\gamma(E_\gamma) = T_\gamma + U_\gamma - E_\gamma, \tag{2.22a}$$

$$E_\gamma = E + \epsilon_\gamma. \tag{2.22b}$$

The potentials U_γ have been chosen to eliminate all diagonal contributions from the residual interactions v, i.e., $\langle \Phi_{\gamma\vec{r}} | \hat{V}_\gamma | \Phi_{\gamma\vec{r}'} \rangle$ vanishes for $\gamma = \alpha, \beta$. This means that U_α and U_β are folded or, more appropriately, averaged distorting potentials given by

$$U_\alpha(\vec{r}_\alpha) = \langle \Phi_{\alpha\vec{r}_\alpha} | V_{Ab} + V_{Ax} | \Phi_{\alpha\vec{r}_\alpha} \rangle, \tag{2.23a}$$

$$U_\beta(\vec{r}_\beta) = \langle \Phi_{\beta\vec{r}_\beta} | V_{Ab} + V_{bx} | \Phi_{\beta\vec{r}_\beta} \rangle. \tag{2.23b}$$

This particular choice of U_γ is uniquely convenient since it simplifies the form of the coupled equations (2.20) and (2.21). The folded potentials serve to define the lowest-order theory and consequently define what is meant by the higher-order corrections. As shown in Ref. 38, use of folded potentials tends to give smaller higher-order effects than would be obtained with arbitrary optical potentials. Each of the coupling kernels can be written in two alternative forms:

$$K_{\alpha\beta}(\vec{r}_\alpha,\vec{r}_\beta) = I_{\alpha\beta}(\vec{r}_\alpha,\vec{r}_\beta) + D_\alpha(E_\alpha)N(\vec{r}_\alpha,\vec{r}_\beta) \tag{2.24a}$$

$$= I_{\beta\alpha}(\vec{r}_\alpha,\vec{r}_\beta) + N(\vec{r}_\alpha,\vec{r}_\beta)D_\beta(E_\beta), \tag{2.24b}$$

$$K_{\beta\alpha}(\vec{r}_\alpha,\vec{r}_\beta) = I_{\beta\alpha}(\vec{r}_\alpha,\vec{r}_\beta) + D_\beta(E_\beta)N(\vec{r}_\alpha,\vec{r}_\beta) \tag{2.25a}$$

$$= I_{\alpha\beta}(\vec{r}_\alpha,\vec{r}_\beta) + N(\vec{r}_\alpha,\vec{r}_\beta)D_\alpha(E_\alpha), \tag{2.25b}$$

where $N(\vec{r}_\alpha,\vec{r}_\beta)$ is the overlap kernel defined by Eq. (2.13),

$$N(\vec{r}_\alpha,\vec{r}_\beta) = J\,\phi_\alpha(\vec{r}_{bx})\phi_\beta(\vec{r}_{Ax}), \tag{2.26}$$

and $I_{\alpha\beta}$ and $I_{\beta\alpha}$ are the *interaction kernels*

$$I_{\alpha\beta}(\vec{r}_\alpha,\vec{r}_\beta) = J\,\phi_\alpha(\vec{r}_{bx})\hat{V}_\alpha\phi_\beta(\vec{r}_{Ax}), \tag{2.27}$$

$$I_{\beta\alpha}(\vec{r}_\alpha,\vec{r}_\beta) = J\,\phi_\beta(\vec{r}_{Ax})\hat{V}_\beta\phi_\alpha(\vec{r}_{bx}). \tag{2.28}$$

The Jacobian J is defined by Eq. (2.15).

In Eqs. (2.24) and (2.25) the terms involving $D_\gamma(E_\gamma)$ and $N(\vec{r}_\alpha, \vec{r}_\beta)$ represent nonorthogonality coupling. These complicated terms have no counterparts in the coupled equations for inelastic scattering. As indicated by Eqs. (2.24) and (2.25), each of the kernels $K_{\alpha\beta}$ and $K_{\beta\alpha}$ can be represented in two alternative ways, corresponding to the two ways of partitioning the full Hamiltonian [Eqs. (2.3) and (2.4)]. From Eq. (2.24) and (2.25) we have

$$\begin{aligned} I_{\alpha\beta} &= I_{\beta\alpha} + N D_\beta(E_\beta) - D_\alpha(E_\alpha)N \\ &= I_{\beta\alpha} + D_\beta(E_\beta)N - N D_\alpha(E_\alpha)\,, \end{aligned} \tag{2.29}$$

which is the post-prior transformation, discussed in Ref. 25. This identity shows that the interaction kernels $I_{\alpha\beta}$ and $I_{\beta\alpha}$ differ by terms proportional to the overlap kernel N. In the limit of orthogonal channel wave functions (i.e., small nonorthogonality effects), $N \to 0$ and Eq. (2.29) yields

$$I_{\alpha\beta} = I_{\beta\alpha} \quad (N=0)\,. \tag{2.30}$$

This result means that the calculation is greatly simplified if all effects of the overlap kernel N can be neglected. In particular, only the simpler of the two kernels $I_{\alpha\beta}$ and $I_{\beta\alpha}$ need be computed. Consequently, it is useful to assess the magnitude of the nonorthogonality effects.

The size of the nonorthogonality effects is determined by comparing calculations using the full MS equations, Eqs. (2.20) and (2.21), with calculations in which the overlap kernel N is replaced by zero. Equation (2.24) and (2.25) indicate that for each kernel the form obtained by setting $N=0$ depends on which expression is used for that kernel. From these alternate definitions, we select Eqs. (2.24b) and (2.25a), which give $K_{\alpha\beta} = K_{\beta\alpha} = I_{\beta\alpha}$. The kernel $I_{\beta\alpha}$ is often more convenient to calculate and also allows for interpretation based on the zero-range approximation. The full MS equations now reduce to

$$D_\alpha(E_\alpha)\bar{\chi}_\alpha(\vec{r}_\alpha) = -\int I_{\beta\alpha}(\vec{r}_\alpha, \vec{r}_\beta)\bar{\chi}_\beta(\vec{r}_\beta)\,d\vec{r}_\beta\,, \tag{2.31}$$

$$D_\beta(E_\beta)\bar{\chi}_\beta(\vec{r}_\beta) = -\int I_{\beta\alpha}(\vec{r}_\alpha, \vec{r}_\beta)\bar{\chi}_\alpha(\vec{r}_\alpha)\,d\vec{r}_\alpha\,. \tag{2.32}$$

Because nonorthogonality has been disregarded in these equations, the functions $\bar{\chi}_\gamma$ differ from the functions χ_γ and give different S-matrix elements $\bar{S}_{\gamma\gamma'}$. The effect of the nonorthogonality terms is then represented by the difference between $\bar{S}_{\gamma\gamma'}$ and $S_{\gamma\gamma'}$ (or corresponding cross sections). We shall refer to Eqs. (2.31) and (2.32) as the symmetric interaction-coupled (SIC) equations, since they involve symmetric coupling kernels.

Kunz[31] has derived a similar, but unsymmetric, set of interaction-coupled (UIC) equations from a different point of view:

$$D_\alpha(E_\alpha)\chi_\alpha^{\mathrm{UIC}}(\vec{r}_\alpha) = -\int I_{\beta\alpha}(\vec{r}_\alpha, \vec{r}_\beta)\chi_\beta^{\mathrm{UIC}}(\vec{r}_\beta)d\vec{r}_\beta)\,, \tag{2.33}$$

$$D_\beta(E_\beta)\chi_\beta^{\mathrm{UIC}}(\vec{r}_\beta) = -\int I_{\alpha\beta}(\vec{r}_\alpha, \vec{r}_\beta)\chi_\alpha^{\mathrm{UIC}}(\vec{r}_\alpha)\,d\vec{r}_\alpha\,. \tag{2.34}$$

These equations differ from Eqs. (2.31) and (2.32) only by terms involving N, as can be seen by Eq. (2.29). Kunz shows that iterating equations (2.33) and (2.34) generates a particular distorted-wave (DW) series, in which only partitions α and β appear, and the intermediate-state sums in each term are truncated to include only one bound state in each partition. This is easily demonstrated by using the Green's functions of $D_\alpha(E_\alpha)$ and $D_\beta(E_\beta)$ to convert Eqs. (2.33) and (2.34) into integral equations, iterating and then inserting this result in an integral expression for the transition amplitude. The resulting DW series has intermediate states with only one bound state in each arrangement. Hence the UIC equations (2.33) and (2.34) are equivalent to a truncation of the set of intermediate states.

In contrast to the UIC equations, the MS method is based on consistent application of quantum mechanics within the definite model space spanned by the set of vectors (2.12). However, both the MS method and the UIC method involve severe truncations of the problem. The two truncations are not equivalent, and so the methods must be regarded as distinct. They may be viewed as alternative models of the reaction. Whether or not their differences are quantitatively significant would have to be decided by numerical calculation. Which method is superior might then be investigated by comparing both with the results of a more accurate method.

For later interpretation of nonorthogonality effects, we now present an extended version of the formulation of the MS method that is due to Udagawa *et al.*,[24] and establish its equivalence to the Ohmura *et al.*[37] formulation. The essential idea of Ref. 24 is to represent Ψ_M by overlap functions $\xi_\gamma(\vec{r})$, defined by

$$\xi_\gamma(\vec{r}) \equiv \langle \Phi_{\gamma\vec{r}} | \Psi_M \rangle\,, \tag{2.35}$$

in place of the coefficient functions $\chi_\gamma(\vec{r})$ that appear in Eq. (2.16). From Eqs. (2.16) and (2.35) the ξ_γ can be expressed in terms of the χ_γ as fol-

lows:

$$\xi_\alpha(\vec{r}_\alpha)=\chi_\alpha(\vec{r}_\alpha)+\int N(\vec{r}_\alpha,\vec{r}_\beta)\chi_\beta(\vec{r}_\beta)d\vec{r}_\beta\,, \quad (2.36)$$

$$\xi_\beta(\vec{r}_\beta)=\chi_\beta(\vec{r}_\beta)+\int N(\vec{r}_\alpha,\vec{r}_\beta)\chi_\alpha(\vec{r}_\alpha)d\vec{r}_\alpha\,. \quad (2.37)$$

Again N is the overlap kernel defined by Eq. (2.13). Because the linear independence of the basis vector depends on properties of N, the overlap kernel is studied in the Appendix. It also appears in the discussion of nonorthogonality effects, Sec. V. We have already noted that N is localized. From Eqs. (2.36) and (2.37) it now follows that ξ_γ and χ_γ agree asymptotically, although they differ at short distances.

Equations (2.36) and (2.37) can be compactly written in terms of matrices whose elements are kernels, as follows:

$$\underline{\xi}=(\underline{1}+\underline{\mathfrak{N}})\underline{\chi}\,, \quad (2.38)$$

where

$$\underline{\xi}\equiv\begin{pmatrix}\xi_\alpha\\ \xi_\beta\end{pmatrix}, \quad \underline{\chi}\equiv\begin{pmatrix}\chi_\alpha\\ \chi_\beta\end{pmatrix}$$

and (2.39)

$$\underline{\mathfrak{N}}\equiv\begin{pmatrix}0 & N\\ N^\dagger & 0\end{pmatrix}.$$

We denote adjoints by daggers, e.g.,

$$N^\dagger(\vec{r},\vec{r}')\equiv N^*(\vec{r}',\vec{r})\,. \quad (2.40)$$

Coupled differential equations for ξ_α and ξ_β follow directly from Eqs. (2.18), (2.19), and (2.35):

$$D_\alpha(E_\alpha)\xi_\alpha(\vec{r}_\alpha)=-\int I_{\alpha\beta}(\vec{r}_\alpha,\vec{r}_\beta)\chi_\beta(\vec{r}_\beta)d\vec{r}_\beta\,, \quad (2.41)$$

$$D_\beta(E_\beta)\xi_\beta(\vec{r}_\beta)=-\int I_{\beta\alpha}(\vec{r}_\alpha,\vec{r}_\beta)\chi_\alpha(\vec{r}_\alpha)d\vec{r}_\alpha\,. \quad (2.42)$$

Substituting Eqs. (2.36) and (2.37), we obtain

$$D_\alpha(E_\alpha)\xi_\alpha=-I_{\alpha\beta}\xi_\beta+I_{\alpha\beta}N^\dagger\chi_\alpha\,, \quad (2.43)$$

$$D_\beta(E_\beta)\xi_\beta=-I^\dagger_{\beta\alpha}\xi_\alpha+I^\dagger_{\beta\alpha}N\chi_\beta\,, \quad (2.44)$$

where conventional operator notation has been used to indicate multiplications of the various kernels. These are the coupled equations of Udagawa *et al.*[24] The terms containing the N kernel are due to the nonorthogonality of the basis.

The presence of both χ_α and ξ_γ in Eqs. (2.43) and (2.44) is inconvenient. We therefore use Eq. (2.38) to eliminate χ_α and χ_β in favor of ξ_α and ξ_β. This requires inversion of the matrix $\underline{1}+\underline{\mathfrak{N}}$ which is discussed in more detail in the Appendix. We have

$$\underline{\chi}=(\underline{1}+\underline{\mathfrak{N}})^{-1}\underline{\xi}\equiv\underline{\Lambda}\,\underline{\xi}\,, \quad (2.45)$$

where the inverse matrix Λ is given by

$$\underline{\Lambda}\equiv\begin{pmatrix}\Lambda_{\alpha\alpha} & \Lambda_{\alpha\beta}\\ \Lambda_{\beta\alpha} & \Lambda_{\beta\beta}\end{pmatrix},$$

$$=\begin{pmatrix}(1-\eta)^{-1} & -(1-\eta)^{-1}N\\ -(1-\tilde{\eta})^{-1}N^\dagger & (1-\tilde{\eta})^{-1}\end{pmatrix}, \quad (2.46)$$

where

$$\eta=NN^\dagger, \quad \tilde{\eta}=N^\dagger N\,. \quad (2.47)$$

Then

$$\chi_\alpha=\Lambda_{\alpha\alpha}\xi_\alpha+\Lambda_{\alpha\beta}\xi_\beta\,,$$
$$\chi_\beta=\Lambda_{\beta\alpha}\xi_\alpha+\Lambda_{\beta\beta}\xi_\beta\,, \quad (2.48)$$

and Eqs. (2.43) and (2.44) become

$$D_\alpha(E_\alpha)\xi_\alpha=-I_{\alpha\beta}(1-N^\dagger\Lambda_{\alpha\beta})\xi_\beta+I_{\alpha\beta}N^\dagger\Lambda_{\alpha\alpha}\xi_\alpha\,, \quad (2.49)$$

$$D_\beta(E_\beta)\xi_\beta=-I^\dagger_{\beta\alpha}(1-N\Lambda_{\beta\alpha})\xi_\alpha+I^\dagger_{\beta\alpha}N\Lambda_{\beta\beta}\xi_\beta\,. \quad (2.50)$$

More briefly,

$$[D_\alpha(E_\alpha)-\mathfrak{U}_\alpha]\xi_\alpha=-\mathcal{G}_{\alpha\beta}\xi_\beta\,, \quad (2.51)$$

$$[D_\beta(E_\beta)-\mathfrak{U}_\beta]\xi_\beta=-\mathcal{G}_{\beta\alpha}\xi_\alpha\,, \quad (2.52)$$

where

$$\mathfrak{U}_\alpha\equiv I_{\alpha\beta}N^\dagger\Lambda_{\alpha\alpha}, \quad \mathfrak{U}_\beta\equiv I^\dagger_{\beta\alpha}N\Lambda_{\beta\beta}\,, \quad (2.53)$$

$$\mathcal{G}_{\alpha\beta}\equiv I_{\alpha\beta}(1-N^\dagger\Lambda_{\alpha\beta}), \quad \mathcal{G}_{\beta\alpha}\equiv I^\dagger_{\beta\alpha}(1-N\Lambda_{\beta\alpha})\,. \quad (2.54)$$

In Eqs. (2.51) and (2.52), the nonlocal kernels $\mathfrak{U}_\alpha$ and $\mathfrak{U}_\beta$ modify the diagonal potentials, while the kernels $\mathcal{G}_{\alpha\beta}$ and $\mathcal{G}_{\beta\alpha}$ represent renormalized interaction kernels.

It is important to stress that the functions ξ_γ and χ_γ are different representations of the model wave function Ψ_M. These two functions give the same S-matrix elements since, as Eqs. (2.36) and (2.37) indicate, they are identical for large r_γ where the S matrix is determined.

We conclude this section by deriving a third formulation of the MS method. This form of the coupled equations provides new insight since in this formulation the nonorthogonality corrections are completely isolated in nonlocal diagonal potentials and do not renormalize the coupling kernels. Starting with Eq. (2.20) we use Eq. (2.24b) to obtain

$$D_\alpha(E_\alpha)\chi_\alpha=-I_{\beta\alpha}\chi_\beta-ND_\beta(E_\beta)\chi_\beta\,. \quad (2.55)$$

Then using Eq. (2.21) yields

$$D_\alpha(E_\alpha)\chi_\alpha=-I_{\beta\alpha}\chi_\beta+NK^\dagger_{\beta\alpha}\chi_\alpha\,, \quad (2.56)$$

or

$$[D_\alpha(E_\alpha)-\mathfrak{V}_\alpha]\chi_\alpha=-I_{\beta\alpha}\chi_\beta\,, \quad (2.57)$$

where $\mathfrak{V}_\alpha$ is a nonlocal interaction defined by

$$\mathcal{U}_\alpha \equiv NK^\dagger_{\beta\alpha}\,. \tag{2.58}$$

Similarly, for channel β we have from Eqs. (2.21), (2.25b), and (2.20)

$$[D_\beta(E_\beta) - \mathcal{U}_\beta]\,\chi_\beta = -\,I^\dagger_{\alpha\beta}\chi_\alpha\,, \tag{2.59}$$

with

$$\mathcal{U}_\beta \equiv N^\dagger K_{\alpha\beta}\,. \tag{2.60}$$

In Eqs. (2.57) and (2.59) the nonorthogonality corrections are now completely separated from the coupling terms and are represented by the nonlocal diagonal potentials $\mathcal{U}_\gamma$ which produce only elastic scattering. Because the corrections do not directly couple the channels, their effect on rearrangement can only be indirect, i.e., of higher order. We comment further on this point in Sec. V.

III. DETAILS OF THE CALCULATION

We direct our attention to quantitative assessment of both nonorthogonality (N kernel) and channel-coupling (I kernel) effects. For this purpose accurate numerical solution of Eqs. (2.20), (2.21), (2.31), and (2.32) is necessary. For simplicity we consider applications in which the two bound states ϕ_α and ϕ_β are s wave. Using standard partial-wave techniques, i.e., expanding χ_α and χ_β in partial waves, Eqs. (2.20) and (2.21) reduce to coupled radial integro-differential equations of the form

$$D_L(E_\alpha)\chi^\alpha_L(r_\alpha) = S^{\alpha\beta}_L(r_\alpha)\,, \tag{3.1}$$

$$D_L(E_\beta)\chi^\beta_L(r_\beta) = S^{\beta\alpha}_L(r_\beta)\,, \tag{3.2}$$

where the differential operator for channel $\gamma(=\alpha$ or $\beta)$ is

$$D_L(E_\gamma) = -\frac{\hbar^2}{2\mu_\gamma}\left[\frac{d^2}{dr_\gamma^2} - \frac{L(L+1)}{r_\gamma^2}\right] + U_\gamma(r_\gamma) - E_\gamma\,. \tag{3.3}$$

The source terms in channels α and β are

$$S^{\alpha\beta}_L(r_\alpha) = -\int_0^\infty K^{\alpha\beta}_L(r_\alpha, r_\beta)\chi^\beta_L(r_\beta)dr_\beta\,, \tag{3.4}$$

$$S^{\beta\alpha}_L(r_\beta) = -\int_0^\infty K^{\beta\alpha}_L(r_\alpha, r_\beta)\chi^\alpha_L(r_\alpha)dr_\alpha\,. \tag{3.5}$$

In Ref. 37 it is shown that $K^{\alpha\beta}_L = K^{\beta\alpha}_L$. Consequently, the same coupling kernel, $K_L(r_\alpha, r_\beta)$, appears in both source terms $S^{\alpha\beta}_L$ and $S^{\beta\alpha}_L$. This kernel is given by

$$K_L(r_\alpha, r_\beta) = \int_{-1}^{1} g(r_\alpha, r_\beta, y)P_L(y)dy\,, \tag{3.6a}$$

$$y = \vec{r}_\alpha \cdot \vec{r}_\beta / r_\alpha r_\beta\,. \tag{3.6b}$$

Here $P_L(y)$ is the Legendre polynomial of order L, and

$$g(r_\alpha, r_\beta, y) = 2\pi J r_\alpha r_\beta\left\{[c + V_{Ab} + d(V_{Ax} + V_{bx})]\phi_\alpha(r_{bx})\phi_\beta(r_{Ax}) + e\,\frac{\vec{r}_{bx}\cdot\vec{r}_{Ax}}{r_{bx}r_{Ax}}\,\frac{d\phi_\alpha(r_{bx})}{dr_{Ax}}\,\frac{d\phi_\beta(r_{Ax})}{dr_{Ax}}\right\}. \tag{3.7}$$

The constants c, d, and e of Eq. (3.7) are defined by

$$c = -\,J^{1/3}\left[\epsilon_\alpha + \frac{bA}{aB}\,\epsilon_\beta\right] - E_\beta\,, \tag{3.8}$$

$$d = \frac{-bA}{x(a+A)}\,, \tag{3.9}$$

$$e = \frac{-\hbar^2 J^{1/3}}{x}\,, \tag{3.10}$$

and ϵ_α and ϵ_β are the binding energies for the $b+x$ and $A+x$ systems. The chosen independent variables are r_α and r_β, in terms of which

$$r_{bx} = J^{1/3}\left[\left(\frac{A}{B}\,r_\alpha\right)^2 + r_\beta^2 - \frac{2A}{B}\,r_\alpha r_\beta y\right]^{1/2}, \tag{3.11}$$

$$r_{Ax} = J^{1/3}\left[r_\alpha^2 + \left(\frac{b}{a}\,r_\beta\right)^2 - \frac{2b}{a}\,r_\alpha r_\beta y\right]^{1/2}, \tag{3.12}$$

$$r_{Ab} = \frac{1}{a+A}[(ar_\alpha)^2 + (Br_\beta)^2 + 2aBr_\alpha r_\beta y]^{1/2}\,. \tag{3.13}$$

Because of the rotational invariance of the kernel and the folded distorting potentials U_α and U_β, the angular momentum L is the same in both channels. Applications requiring non-s-wave bound states introduce the additional complications entailed by coupling of different L values.

The folded distorting potentials U_α and U_β are given by

$$U_\alpha(r_\alpha) = \int_0^\infty V_\alpha(r_\alpha, r_{bx})\,|\phi_\alpha(\vec{r}_{bx})|^2 r_{bx}^2 dr_{bx}\,, \tag{3.14}$$

with

$$V_\alpha(r_\alpha, r_{bx}) = 2\pi\int_{-1}^{1}[V_{Ab}(r_{Ab}) + V_{Ax}(r_{Ax})]dz\,. \tag{3.15}$$

The following relations apply in the integrand:

$$r_{Ab} = \left[r_\alpha^2 + \left(\frac{x}{a}\,r_{bx}\right)^2 - \frac{2x}{a}\,r_\alpha r_{bx} z\right]^{1/2}, \tag{3.16}$$

$$r_{Ax} = \left[r_\alpha^2 + \left(\frac{b}{a}\,r_{bx}\right)^2 + \frac{2b}{a}\,r_\alpha r_{bx} z\right]^{1/2}. \tag{3.17}$$

For the β channel

$$U_\beta(r_\beta) = \int_0^\infty V_\beta(r_\beta, r_{Ax}) \left| \phi_\beta(r_{Ax}) \right|^2 r_{Ax}^2 dr_{Ax} , \tag{3.18}$$

with

$$V_\beta(r_\beta, r_{Ax}) = 2\pi \int_{-1}^{1} [V_{Ab}(r_{Ab}) + V_{bx}(r_{bx})] dz , \tag{3.19}$$

$$r_{Ab} = \left[r_\beta^2 + \left(\frac{x}{B} r_{Ax} \right)^2 + 2 \frac{x}{B} r_\beta r_{Ax} z \right]^{1/2} , \tag{3.20}$$

$$r_{bx} = \left[r_\beta^2 + \left(\frac{A}{B} r_{Ax} \right)^2 - 2 \frac{A}{B} r_\beta r_{Ax} z \right]^{1/2} . \tag{3.21}$$

These interactions, Eqs. (3.14) and (3.18), do not appear explicitly in the equation for the full kernel, Eq. (3.7). They do, however, affect the interaction kernel, since (in the post form) we have

$$I_L^{\beta\alpha}(r_\alpha, r_\beta) = \int_{-1}^{1} h(r_\alpha, r_\beta, y) P_L(y) dy , \tag{3.22}$$

$$h(r_\alpha, r_\beta, y) = 2\pi J r_\alpha r_\beta [V_{Ab}(r_{Ab}) + V_{bx}(r_{bx}) - U_\beta(r_\beta)] \times \phi_\alpha(r_{bx}) \phi_\beta(r_{Ax}) . \tag{3.23}$$

When we perform the calculations without the overlap kernel N, we replace $K_L^{\alpha\beta}$ in Eqs. (3.4) and (3.5) by $I_L^{\beta\alpha}$ defined by Eqs. (3.22) and (3.23).

Statement of the boundary conditions completes the specification of the desired solution. When α is the incident channel, we require asymptotically

$$\chi_L^\alpha(r_\alpha) = F_L^\alpha(r_\alpha) + T_L^{\alpha\alpha} H_L^\alpha(r_\alpha) , \tag{3.24}$$

$$\chi_L^\beta(r_\beta) = T_L^{\beta\alpha} H_L^\beta(r_\beta) , \tag{3.25}$$

where $H_L^\gamma(r_\gamma)$ is a purely outgoing wave in channel γ,

$$H_L^\gamma(r_\gamma) = G_L^\gamma(r_\gamma) + i F_L^\gamma(r_\gamma) , \tag{3.26}$$

and F_L^γ and G_L^γ are the regular and irregular Coulomb functions, respectively. The quantities $T_L^{\alpha\alpha}$ and $T_L^{\beta\alpha}$ are the partial-wave transition amplitudes for the elastic ($\alpha \to \alpha$) and rearrangement ($\alpha \to \beta$) processes. Equations (3.24) and (3.25) are the appropriate boundary conditions for the two specific processes $A(a,a)A$ and $A(a,b)B$. When β is the incident channel, corresponding to the time reversed reactions $B(b,b)B$ and $B(b,a)A$, we have different boundary conditions:

$$\chi_L^\alpha(r_\alpha) = T_L^{\alpha\beta} H_L^\alpha(r_\alpha) , \tag{3.27}$$

$$\chi_L^\beta(r_\beta) = F_L^\beta(r_\beta) + T_L^{\beta\beta} H_L^\beta(r_\beta) . \tag{3.28}$$

An interative procedure was used to solve the coupled equations (3.1) and (3.2). For definiteness, assume particle a is incident on target A. The first step of the iterative procedure is to obtain the homogeneous solution of Eq. (3.1), subject to the boundary condition Eq. (3.24). This zeroth-order solution is inserted in Eq. (3.5) and the approximate source term $S_L^{\beta\alpha}$ is then used in Eq. (3.2). This equation is now uncoupled but is inhomogeneous, so the general solution consists of a constant times the homogeneous solution plus the particular solution of the full equation. The constant in this general solution must be chosen to satisfy the outgoing boundary condition, Eq. (3.25), from which the lowest-order transfer amplitude is obtained. This same procedure is now repeated for the elastic channel, but now Eq. (3.4) and boundary condition (3.24) are used and the entire cycle is continued. The process is terminated when the difference between amplitudes from successive iterations is less than 1%. In all our numerical calculations this degree of convergence required five iterations or less. It is possible that convergence may be less rapid in cases with more channels.

Finally, we point out that our calculations use finite-range interactions throughout and correctly include target recoil. The results of the calculations are presented and discussed in the next section.

IV. EMPIRICAL STUDY OF NONORTHOGONALITY AND CHANNEL-COUPLING EFFECTS

We have applied the MS method to several light-ion- and heavy-ion-induced reactions at various energies with different targets and projectiles. The calculations were performed for the reactions (d,d), (d,p), and (p,p) on ^{16}O and ^{90}Zr targets, and for the reactions ^{28}Si(^{16}O, ^{16}O) ^{28}Si and ^{28}Si(^{16}O, ^{12}C) ^{32}S (treated as a four-particle-cluster transfer). We have also conducted an empirical study of the sensitivity of nonorthogonality and channel-coupling effects to variations in model parameters, in an effort to understand the nature of these effects.

The results for the reactions ^{16}O$(d,d)^{16}$O, ^{16}O$(d,p)^{17}$O, and ^{17}O$(p,p)^{17}$O at lab energies $E_d = 10.49$ MeV and $E_p = 10.98$ MeV are presented in Figs. 2–5. A preliminary report of these calculations has previously been published.[29] The parameters specifying the interactions are given in Table I. Figure 2 displays the behavior of the radial kernel K_L for several partial waves in the ^{16}O$(d,d)^{16}$O, ^{16}O$(d,p)^{17}$O, and ^{17}O$(p,p)^{17}$O reactions with and without nonorthogonality contributions. The angular distributions for these processes are shown in Figs. 3–5. In these figures the solid and dashed curves represent the coupled-channels results using the full kernel K_L and interaction kernel $I_L^{\beta\alpha}$, respectively. The difference between these two curves constitutes the effect

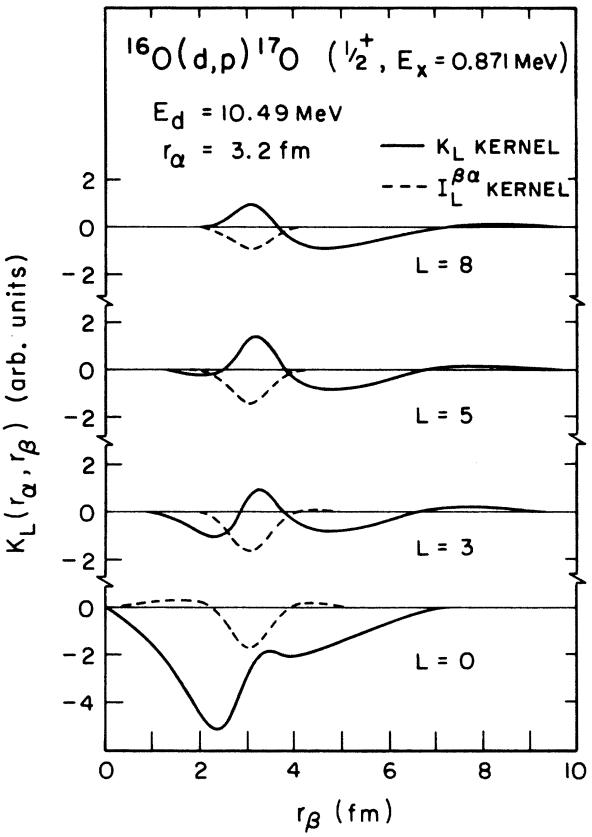

FIG. 2. Comparison of the full (solid curve) and interaction (dashed curve) partial-wave kernels for $^{16}O(d,p)^{17}O$ at E_d(lab) = 10.49 MeV.

of channel nonorthogonality. To assess the channel-coupling effect (i.e., that produced by the interaction kernel alone), the dashed curve should be compared with the dotted curve which represents the cross section without coupling.

The key results of the calculations are as follows: (i) though the contribution of nonorthogonality to the kernel is large, it results in much smaller effects in the cross sections; (ii) the interaction kernel produces a much larger channel-coupling effect in (p,p) than in either (d,d) or (d,p); (iii) the nonorthogonality corrections are larger in (d,d) and (d,p) than in (p,p); (iv) for (d,d) and (d,p) there is destructive interference between nonorthogonality effects and channel coupling effects, but for (p,p) the interference is constructive.

We have varied several parameters of the model in an effort to understand the nature of these effects. First, the dependence of the results on target mass was explored by replacing ^{16}O by a heavier target, ^{90}Zr. This change greatly reduced both coupling and nonorthogonality effects, as indicated in Figs. 6 and 7, but the qualitative

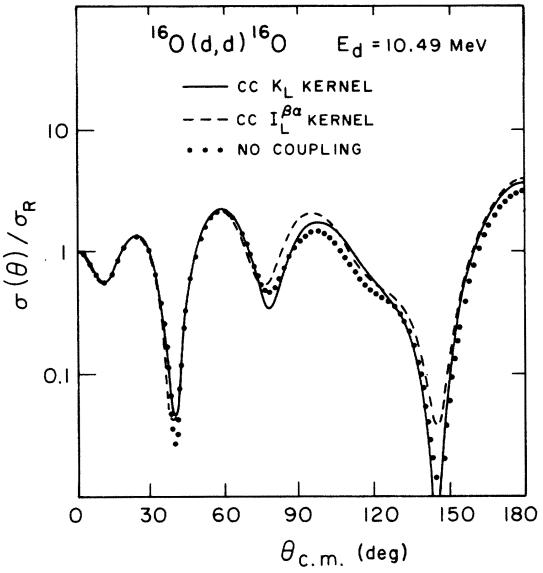

FIG. 3. Ratio of elastic scattering to Rutherford for $^{16}O(d,d)^{16}O$ with contributions from an intermediate proton channel. Coupled-channels (CC) calculations were performed with E_d(lab) = 10.49 MeV. The calculations treat finite range, target recoil, and channel nonorthogonality exactly, and use folded distorting potentials.

results i–iv were unaltered.

Second, we investigated the dependence of the nonorthogonality corrections on the total energy, which could be produced by the explicit E_α dependence in Eqs. (3.7) and (3.8). Calculations for the $^{16}O(d,d)^{16}O$ and $^{16}O(d,p)^{17}O$ reactions, with

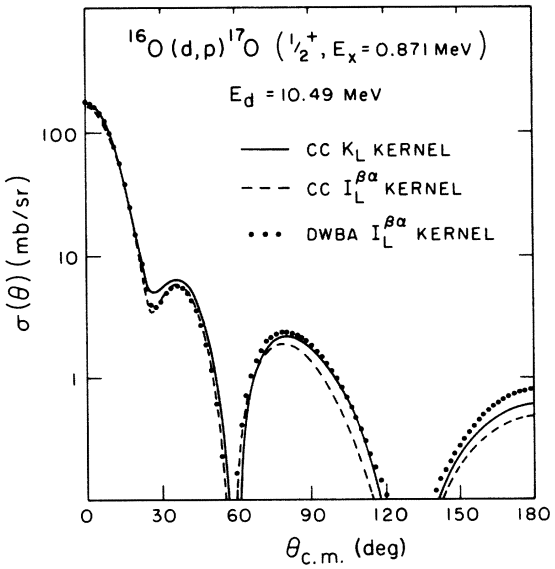

FIG. 4. Comparison of CC with DWBA calculation using folded distorting potentials for $^{16}O(d,p)^{17}O$.

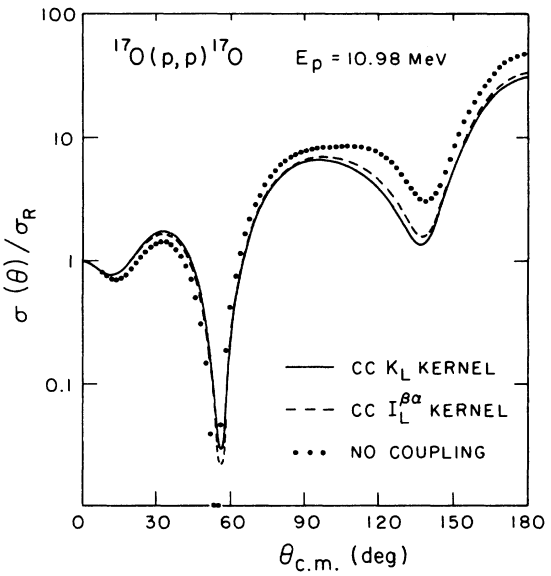

FIG. 5. Ratio of elastic scattering to Rutherford for $^{17}O(p,p)^{17}O$, showing contribution from an intermediate deuteron channel. The total energy is the same as in the $^{16}O(d,d)^{16}O$ and $^{16}O(d,p)^{17}O$ reactions of Figs. 2–4.

values of E_α corresponding to laboratory energies $E_d = 14.8$ and 20 MeV, are displayed in Figs. 8, 9, and 10. The dependence on the total energy is evidently rather weak. The energies ϵ_α and ϵ_β of the bound states are actually fixed by the choice of the projectile (here a deuteron) and the final nuclear state. However, we can vary these energies by altering the depths of the potentials V_{bx} and V_{Ax}, and still maintain energy conservation. The results are strongly sensitive to the deuteron binding energy ϵ_α. Increasing ϵ_α from 2.225 to 6.68 MeV enhances the channel-coupling effect produced by the interaction kernel by approximately 20% for $^{17}O(p,p)^{17}O$ and 12% for $^{16}O(d,p)^{17}O$. This increase in the multistep amplitude with increasing ϵ_α is due to the associated increase in potential strength of V_{bx}. The same parameter variation also enhanced the nonorthogonality effect by 10% for $^{17}O(p,p)^{17}O$ and by 6% for $^{16}O(d,p)^{17}O$. Changing the neutron binding energy, however, from $\epsilon_\beta = 3.27$ to 9.81 MeV reduced the size of both N-kernel and I-kernel effects. This reduction was small, typically of the order of 5%.

Increasing the absorption strength W_{Ab} from 9.24 to 13.86 MeV reduced both the I-kernel and N-kernel higher-order effects by about 5%. Finally, a slight enhancement in effects was obtained when W_{Ab} was decreased to 4.62 MeV.

A detailed examination of all parameter variations has indicated two general trends. First, the nonorthogonality (N-kernel) effect is important only when the channel-coupling (I-kernel) effect is important. Secondly, there is a strong correlation between the size of the higher-order effects and the size of the transfer amplitude, i.e., parameter changes that increase $T_L^{\beta\alpha}$ also enhance the higher-order corrections, and vice versa. In Secs. V and VII theoretical explanations are given for these empirical results.

Of special interest are heavy-ion reactions, which involve strong absorption and many partial waves. Application was made to the reactions $^{28}Si(^{16}O, ^{16}O)^{28}Si$ and $^{28}Si(^{16}O, ^{12}C)^{32}S$ (ground state) at $E_\alpha = 42$ MeV (lab). In our simple three-body model the four transferred nucleons are treated as an inert cluster, an α particle. Now, in contrast to the (d,p) calculations it is no longer realistic to assume unit spectroscopic factor, since in four-particle transfer the cluster parentages are not as large. Accordingly, the coupling kernel

TABLE I. Pair potentials V_{ij} for light-ion-induced reaction calculation. For the $p+n$ system the interaction is Gaussian, $-Ve^{-X_R^2}$, $X_R = r/a_R$. For the remaining pairs the real interactions are of Woods-Saxon form, $-V(1+e^{X_R})^{-1}$, $X_R = (r - r_R A_j^{1/3})/a_R$, and the imaginary interactions (where appropriate) are Woods-Saxon derivatives, $-4We^{X_I}(1+e^{X_I})^{-2}$, $X_I = (r - r_I A_j^{1/3})/a_I$. The parameters are taken from Ref. 45. Distorting potentials U_α and U_β are obtained by folding.

Pair $i+j$	Relative energy (MeV)	V (MeV)	r_R (fm)	a_R (fm)	W (MeV)	r_I (fm)	a_I (fm)	r_c (fm)
$p+n$	−2.225	72.71	···	1.48	···	···	···	···
$n+^{16}O$	−3.27	54.54	1.25	0.65	···	···	···	···
$n+^{90}Zr$	−6.00	67.46	1.25	0.65	···	···	···	···
$p+^{16}O$ / $n+^{16}O$	$\frac{1}{2}E_d = 4.66$	45.56	1.31	0.66	9.24	1.26	0.48	1.31
$p+^{90}Zr$ / $n+^{90}Zr$	$\frac{1}{2}E_d = 5.87$	45.34	1.28	0.66	9.20	1.25	0.48	1.28

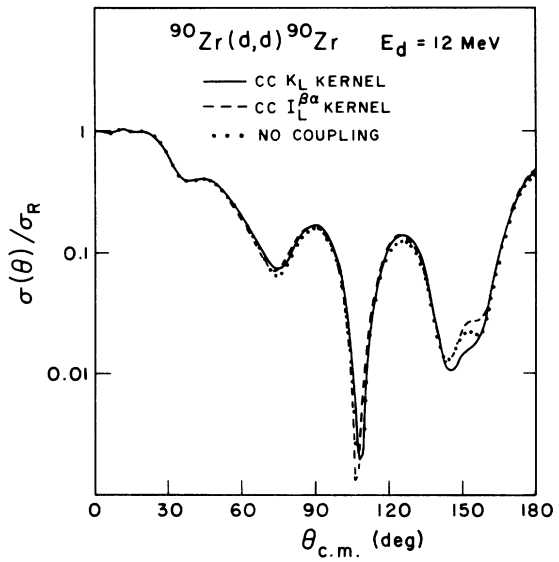

FIG. 6. Ratio of elastic scattering to Rutherford for ^{90}Zr$(d,d)^{90}$Zr, at E_d(lab) = 12 MeV.

must be multiplied by a factor $S_{\alpha\beta}{}^{1/2}$ defined by

$$S_{\alpha\beta}{}^{1/2} \equiv [S_\alpha(bx)S_\beta(Ax)]^{1/2}, \tag{4.1}$$

where $S_\alpha(bx)$ and $S_\beta(Ax)$ are the spectroscopic factors for the $b+x$ and $A+x$ systems, respectively. The spectroscopic factors now influence the dynamics instead of entering simply as normalization constants, as in DWBA. The heavy-ion calculations were performed with the parameters listed in Table II. The computed angular distributions revealed extremely small, less than 5%,

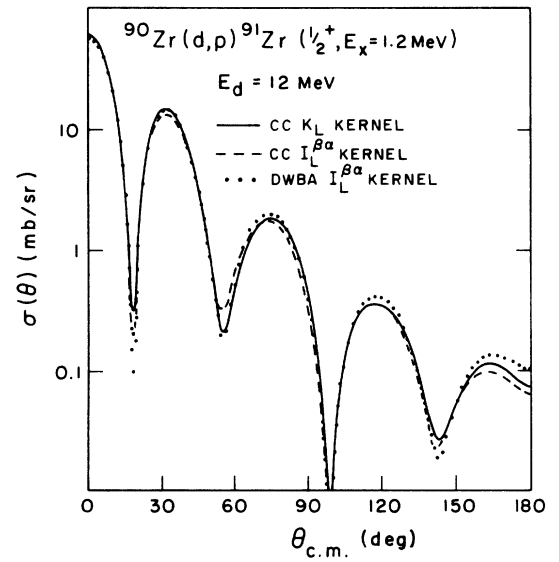

FIG. 7. Comparison of CC and DWBA calculations for ^{90}Zr$(d,p)^{91}$Zr, at E_d(lab) = 12 MeV.

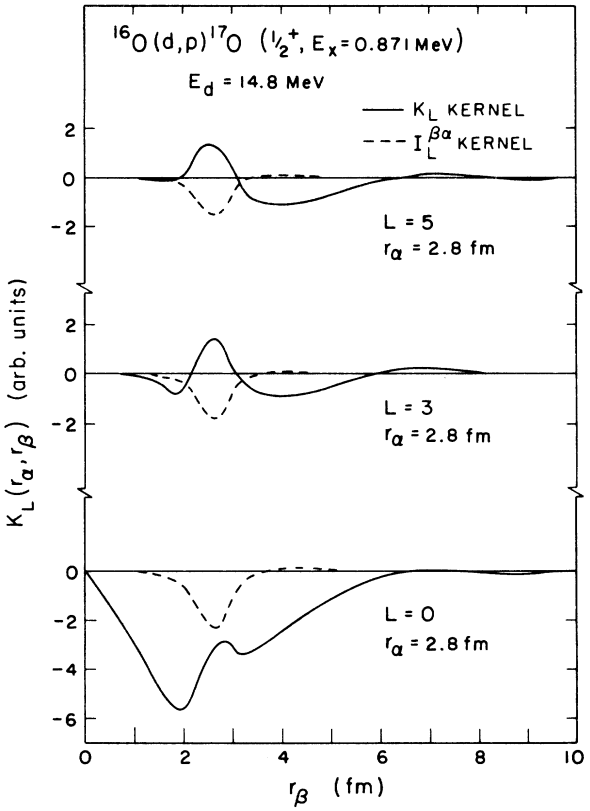

FIG. 8. Comparison of the full (solid curve) and interaction (dashed curve) partial-wave kernels for ^{16}O$(d, p)^{17}$O at E_d (lab) = 14.8 MeV.

higher-order effects. Because the effects were so small we have not plotted these cross sections.

To explore possible explanations for this small effect, we have made a number of other heavy-ion calculations. Increasing $S_{\alpha\beta}{}^{1/2}$ from 0.5 to 2.0 still does not generate appreciable higher-order effects. Variation of model parameters, as in (d, p), indicated again a correlation between the magnitude of higher-order effects and rearrangement amplitudes. Both the existence of this relation and the size of higher-order effects are consistent with the fact that the (^{16}O, ^{12}C) partial wave amplitude is much smaller than the (d, p) amplitude. We again postpone full theoretical explanation until Sec. V.

Our calculations indicate that higher-order effects are small for (^{16}O, ^{16}O) and (^{16}O, ^{12}C). However, from our analysis of these reactions, a new type of effect, which occurs primarily in lowest order, is seen to be important. This involves the optical remnant term $(V_{Ab} - U_\beta)$ of the residual interaction $\hat{V}_\beta$, Eq. (2.6), which appears in the interaction kernel. This term is neglected in most DWBA calculations. Figure 11 compares calculations with (solid curve) and without (dashed

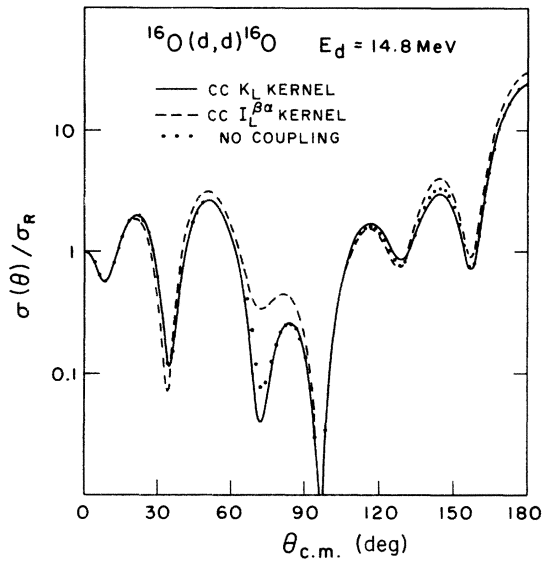

FIG. 9. Ratio of elastic scattering to Rutherford for $^{16}O(d,p,d)^{16}O$ at E_d(lab) = 14.8 MeV.

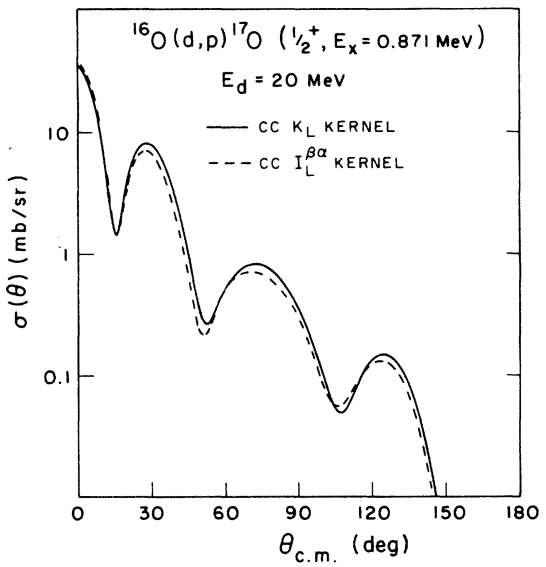

FIG. 10. Comparison of CC calculation with and without nonorthogonality corrections for $^{16}O(d,p)^{17}O$ at E_d(lab) = 20 MeV.

curve) the optical remnant term. The remnant corrections produce a 50% increase in the differential cross section at forward angles and approximately a 30% decrease at back angles. This correction does not improve agreement with experiment[40] (the dotted curve), perhaps because the optical potential used was determined in part by fitting (^{16}O, ^{12}C) data in this mass region, and in those calculations the kernel did not include the optical remnant.

The optical remnant is important for (^{16}O, ^{12}C) because Coulomb effects are important and two units of charge are transferred, so that $Z_A Z_b$ and $Z_B Z_b$ are appreciably different.

DeVries, Satchler, and Kramer[41] have previously discussed the optical remnant and reported sizable effects for single-charge transfer; they indicate that caution should be exercised in neglecting the optical remnant. This is in sharp contrast to (d,p) stripping, where these terms cancel very effectively.

We conclude this section by summarizing the results of our numerical investigations. The effects of channel nonorthogonality are in general small, but can be important when the effects of channel coupling via the I kernel are large. The channel-coupling effects are small for heavy-ion-induced reactions, but for processes involving light projectiles the effects are much larger. These corrections are more important for elastic scattering than for rearrangement. The reaction $^{17}O(p,p)^{17}O$ showed the largest channel-coupling effects. Parameter variations showed that both higher-order effects are correlated with the be-

TABLE II. Pair potentials V_{ij} for heavy-ion-induced reaction calculations. All interactions are of Woods-Saxon form. For the α+ core systems the radius parameter is given by $r_0 A_j^{1/3}$. For the remaining pairs the radius parameter is given by $r_0(A_i^{1/3}+A_j^{1/3})$. Here r_0 is either r_R, r_I, or r_c. The parameters are taken from Ref. 46. Folded potentials are not used in the heavy-ion-induced reaction calculations.

Pair $i+j$	Relative energy (MeV)	V (MeV)	r_R (fm)	a_R (fm)	W (MeV)	r_I (fm)	a_K (fm)	r_c (fm)
$\alpha+^{12}C$	−7.16	72.98	1.25	0.65	...	...	...	1.25
$\alpha+^{28}Si$	−6.95	105.82	1.25	0.65	...	...	...	1.25
$^{12}C+^{28}Si$	20.04	37.00	1.35	0.40	78.00	1.29	0.17	1.35
$^{12}C+^{32}S$	26.52	37.00	1.35	0.40	78.00	1.29	0.17	1.35
$^{16}O+^{28}Si$	26.73	37.00	1.35	0.40	78.00	1.29	0.17	1.35

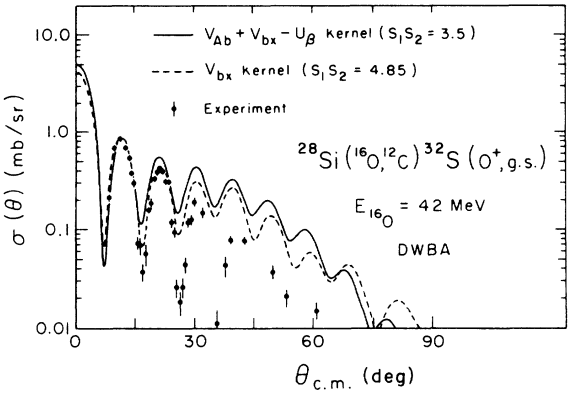

FIG. 11. Comparison of DWBA calculations, with and without the optical remnant term, and experiment for the reaction $^{28}Si(^{16}O,^{12}C)^{32}S$ at E_{lab} = 42 MeV. Experimental data points provided by Peng and Maher, University of Pittsburgh.

havior of the transfer amplitude, a quantity which is quite familiar and well understood. Finally, our calculations have shown that for heavy-ion processes large effects occur, mainly in first order, if the optical remnant term is omitted from the kernel.

V. INTERPRETATION OF NONORTHOGONALITY EFFECTS

In this section we present a theoretical analysis of effects due to the overlap kernel N in Eqs. (2.24), (2.25), (2.53), (2.54), (2.58), and (2.60). Theoretical discussion of the channel-coupling effect produced by the interaction kernel is conducted separately in Sec. VII.

As pointed out in Sec. II, the overlap kernel N contains all geometric information regarding channel nonorthogonality. Hence, an understanding of the nonorthogonality effects can be obtained by studying this kernel in detail. In particular, we wish to use the properties of N to explain why these effects are small for the (d, p) and (^{16}O, ^{12}C) reactions, as the results of Sec. IV indicate. Another aim is to predict where nonorthogonality effects might be important.

We begin with Eqs. (2.57)–(2.60) in which the overlap kernel enters only through the nonorthogonality-induced diagonal terms $\mathfrak{U}_\alpha$ and $\mathfrak{U}_\beta$, defined in Eqs. (2.58) and (2.60):

$$\mathfrak{U}_\alpha = NK^\dagger_{\beta\alpha}, \tag{5.1}$$

$$\mathfrak{U}_\beta = N^\dagger K_{\alpha\beta}. \tag{5.2}$$

Clearly if N is negligible then $\mathfrak{U}_\gamma = 0$ and nonorthogonality does not contribute. To understand what happens when N is not zero, we work in a partial-wave representation and expand $\mathfrak{U}_\gamma$ in Legendre polynomials:

$$\mathfrak{U}_\gamma(\vec{r}_\gamma, \vec{r}'_\gamma) = \sum_L \frac{(2L+1)}{4\pi} \frac{\mathfrak{U}^\gamma_L(r_\gamma, r'_\gamma)}{r_\gamma r'_\gamma} P_L(\hat{r}_\gamma \cdot \hat{r}'_\gamma). \tag{5.3}$$

Now the radial coupled equation for channel α, for example, is

$$D_L(E_\alpha)\chi^\alpha_L(r_2) - \int_0^\infty \mathfrak{U}^\alpha_L(r_\alpha, r'_\alpha)\chi^\alpha_L(r'_\alpha)dr'_\alpha = -\int_0^\infty I^{\alpha\beta}_L(r_\alpha, r_\beta)\chi^\beta_L(r_\beta)dr_\beta, \tag{5.4}$$

where the nonorthogonality-induced potential $\mathfrak{U}^\alpha_L(r_\alpha, r'_\alpha)$ has the form

$$\mathfrak{U}^\alpha_L(r_\alpha, r'_\alpha) = 2\pi r_\alpha r'_\alpha \int_{-1}^{1} \mathfrak{U}_\alpha(r_\alpha, r'_\alpha, y)P_L(y)dy, \tag{5.5}$$

with

$$\mathfrak{U}_\alpha(r_\alpha, r'_\alpha, y) = \int N(\vec{r}_\alpha, \vec{r}_\beta)K_{\beta\alpha}(\vec{r}'_\alpha, \vec{r}_\beta)d\vec{r}_\beta. \tag{5.6}$$

If we also make Legendre expansions for $K_{\beta\alpha}$ and N,

$$K_{\beta\alpha}(\vec{r}_\alpha, \vec{r}_\beta) = \sum_L \frac{(2L+1)}{4\pi} \frac{K_L(r_\alpha, r_\beta)}{r_\alpha r_\beta} P_L(\hat{r}_\alpha \cdot \hat{r}_\beta), \tag{5.7}$$

$$N(\vec{r}_\alpha, \vec{r}_\beta) = \sum_L \frac{(2L+1)}{4\pi} \frac{N_L(r_\alpha, r_\beta)}{r_\alpha r_\beta} P_L(\hat{r}_\alpha \cdot \hat{r}_\beta), \tag{5.8}$$

Eq. (5.5) reduces to

$$\mathfrak{U}^\alpha_L(r_\alpha, r'_\alpha) = \int_0^\infty N_L(r_\alpha, r_\beta)K_L(r'_\alpha, r_\beta)dr_\beta. \tag{5.9}$$

To investigate the strength and range of nonlocality of $\mathfrak{U}^\gamma_L$ as a function of L, we study the eigenfunction expansion of $\mathfrak{U}^\gamma_L$. For this purpose we need the eigenvalues and eigenfunctions u^γ_{Ln} and h^γ_{Ln} of the operator $\mathfrak{U}^\gamma_L$ ($\gamma = \alpha, \beta$), i.e.,

$$\mathfrak{U}^\gamma_L h^\gamma_{Ln} = \int_0^\infty \mathfrak{U}^\gamma_L(r_\gamma, r'_\gamma)h^\gamma_{Ln}(r'_\gamma)dr'_\gamma = u^\gamma_{Ln}h^\gamma_{Ln}. \tag{5.10}$$

We have obtained u^γ_{Ln} and h^γ_{Ln} for $\alpha = d + ^{16}O$ at E_d = 10.49 MeV by diagonalizing the interactions $\mathfrak{U}^\alpha_L$ and $\mathfrak{U}^\beta_L$. We have neglected the imaginary parts of these two nonlocal potentials which are small compared with their real parts. The first few eigenvalues of $\mathfrak{U}^\alpha_L$ and $\mathfrak{U}^\beta_L$ are given in Table III. The eigenfunctions are slowly varying and surface peaked. The range of the nonlocality is about the size of the target nucleus, ^{16}O. The decrease

TABLE III. The four largest eigenvalues u^p_{Ln} and u^d_{Ln} of the nonlocal potentials $\mathfrak{U}^p_L$ and $\mathfrak{U}^d_L$ for each L.

L \ n	u^p_{Ln} 0	1	2	3	u^d_{Ln} 0	1	2	3
0	10.52	3.57	0.72	−0.31	10.39	3.76	0.78	−0.34
1	5.27	1.38	0.33	0.21	5.08	1.50	0.24	−0.07
2	1.99	0.44	−0.34	−0.08	1.85	0.45	0.11	−0.03
3	0.52	−0.33	−0.10	0.09	0.45	−0.16	0.07	−0.04
4	−0.31	−0.12	0.10	−0.05	− 0.22	0.09	−0.07	−0.01
5	−0.29	−0.10	−0.04	−0.02	− 0.20	−0.08	−0.05	−0.02
6	−0.23	−0.07	−0.03	−0.01	− 0.15	−0.05	−0.04	−0.01
7	−0.17	−0.04	−0.03	−0.01	− 0.11	−0.03	−0.01	−0.00
8	−0.12	−0.02	−0.01	−0.00	− 0.08	−0.02	−0.00	−0.00
9	−0.08	−0.01	−0.00	−0.00	− 0.05	−0.01	−0.00	−0.00

of u^γ_{Ln} with n suggests that for each L, $\mathfrak{U}^\alpha_L$ and $\mathfrak{U}^\beta_L$ could be well approximated by separable potentials of rank three or four.

We measure the strength of the nonlocal potentials $\mathfrak{U}^\gamma_L$ by the maximum eigenvalue u^γ_{L0}, for each L. Table III indicates that the strength decreases rapidly with increasing L. The rapid fall with L explains why only the low partial waves ($L=0, 1, 2$) are appreciably influenced by the nonorthogonality correction in our calculations for $^{16}O(d, d)^{16}O$, $^{16}O(d, p)^{17}O$, and $^{17}O(p, p)^{17}O$. However, these partial waves are strongly absorbed and contribute very little. For $E_d = 10.49$ MeV most of the cross section comes from the surface partial waves, $L=3$, 4, and 5. Consequently the cross section is almost unaffected by the nonorthogonality term.

The nonorthogonality-induced potentials $\mathfrak{U}^\alpha_L$ and $\mathfrak{U}^\beta_L$ may also be represented by equivalent local potentials $\bar{\mathfrak{U}}^\alpha_L$ and $\bar{\mathfrak{U}}^\beta_L$. The size of the equivalent local potential provides a more familiar measure of the strength of nonorthogonality effects. We define equivalent local potentials $\bar{\mathfrak{U}}^\gamma_L$ by

$$\bar{\mathfrak{U}}^\gamma_L(r_\gamma)\chi^\gamma_L(r_\gamma) \equiv \int \mathfrak{U}^\gamma_L(r_\gamma, r'_\gamma)\chi^\gamma_L(r'_\gamma)dr'_\gamma, \qquad (5.11)$$

where χ^γ_L is the radial distorted partial wave in channel γ. Unfortunately, $\bar{\mathfrak{U}}^\gamma_L$ has a pole when χ^γ_L has a zero. Since one could smooth out such singularities, we simply disregard them. We have calculated the real parts of the nonorthogonality-induced equivalent local potentials. These potentials are weak, long-ranged, predominantly attractive, and (as mentioned above) decrease rapidly with increasing L value. For example, the depth of the deuteron potential is only 0.65 MeV (real) and 0.26 MeV (imaginary) for the surface partial wave $L=4$; it is not surprising that nonorthogonality corrections have little effect on the cross section for the (d, d) reaction. The same analysis for the proton channel yields quite similar results.

The problem of understanding channel nonorthogonality effects has now been reduced to explaining why the nonorthogonality-induced potentials $\mathfrak{U}^\gamma_L$ fall off rapidly with L. As shown in Sec. IV, the full kernel K_L decreases only slowly with L. Hence it must be the overlap kernel N_L which is mainly responsible for the rapid decrease of $\mathfrak{U}^\gamma_L$. We therefore concentrate on this quantity.

A useful measure of the magnitude of N_L is the uniform norm $\|N_L\|$, which is defined as the square root of the maximum eigenvalue of the operator $N_L N_L^\dagger$. Several properties of this norm are discussed in the Appendix. We have obtained the eigenvalues of $N_L N_L^\dagger$ by numerical diagonalization. They can fairly accurately be represented by the empirical formula

$$\lambda_{Ln} = s t^L p^n, \qquad (5.12)$$

where the three constants are

$$s = 0.37, \quad t = 0.59, \quad p = 0.45. \qquad (5.13)$$

This exponential behavior gives a very rapid falloff of strength with L. In fact, $\|N_L\| \simeq 0.61(0.77)^L$ which gives, for example, $\|N_{L=4}\| = 0.21$. This explains why the nonorthogonality-induced potentials are appreciable only for the low partial waves $L=0, 1, 2$.

It is now appropriate to try to understand why the norm of N_L has the particular behavior described. A first step in this direction is to compute the trace of $NN^\dagger$, which gives a sum rule satisfied by the eigenvalues of $NN^\dagger$:

$$\mathrm{tr}(NN^\dagger) = \sum_L \mathrm{tr}(N_L N_L^\dagger) = \sum_{Ln} (2L+1)\lambda_{Ln}. \qquad (5.14)$$

The factor $2L+1$ is due to the degeneracy implied by rotational invariance. Because the eigenvalues are nonnegative, the partial trace for fixed

L gives an upper bound on the norm of N_L:

$$\| N_L \| = (\lambda_{L0})^{1/2} \leq \left(\sum_n \lambda_{Ln} \right)^{1/2} . \tag{5.15}$$

Since λ_{Ln} decreases rapidly with n, this bound is close enough to $\| N_L \|$ to give quite a useful estimate. These partial traces unfortunately do not seem easy to compute in the general case. However, for the complete trace, we easily find a general result:

$$\begin{aligned} \mathrm{tr}(NN^\dagger) &= \int\int N(\vec{r}_\alpha, \vec{r}_\beta) N(\vec{r}_\alpha, \vec{r}_\beta) d\vec{r}_\alpha d\vec{r}_\beta , \\ &= J^2 \int\int |\phi_\alpha(\vec{r}_{bx})|^2 |\phi_\beta(\vec{r}_{Ax})|^2 d\vec{r}_\alpha d\vec{r}_\beta , \\ &= J \int |\phi_\alpha(r_{bx})|^2 d\vec{r}_{bx} \int |\phi_\beta(\vec{r}_{Ax})|^2 d\vec{r}_{Ax} \\ &= J. \end{aligned} \tag{5.16}$$

By Eqs. (5.14), (5.15), and (5.16), the Jacobian determines an overall scale for the magnitude of the nonorthogonality terms. We might therefore expect nonorthogonality effects to be more important for reactions having large Jacobians, i.e., reactions in which a small mass is transferred from a heavy-ion projectile incident to a heavy target. However, even for these reactions large nonorthogonality effects might be possible only if the decrease of λ_{Ln} with L is sufficiently slow, so that the surface partial waves can be affected. We therefore investigate the L dependence to understand when large effects are possible.

The L dependence of the radial overlap kernel arises from the Legendre expansion, Eq. (5.8):

$$N_L(r_\alpha, r_\beta) = 2\pi r_\alpha r_\beta \int_{-1}^{1} N(r_\alpha, r_\beta, y) P_L(y) dy. \tag{5.17}$$

Equation (5.17) indicates that a rapid decrease with L will occur if the overlap kernel is a slowly varying function of the angle between the channel radii $\vec{r}_\alpha$ and $\vec{r}_\beta$. In fact, if $N(r_\alpha, r_\beta, y)$ is independent of $y = \hat{r}_\alpha \cdot \hat{r}_\beta$, only s waves are affected by nonorthogonality corrections. Conversely, if N is not a smooth function of y we expect many partial waves to contribute, though each contribution may be small, because of the constraint implied by Eqs. (5.14) and (5.15).

To gauge the rapidity of the angle dependence, we differentiate N with respect to y holding r_α and r_β constant. From Eqs. (2.26), (3.11), and (3.12) we obtain

$$\begin{aligned} \left(\frac{\partial N}{\partial y} \right)_{r_\alpha, r_\beta} &= J \left[\frac{d\phi_\alpha}{dr_{bx}} \left(\frac{\partial r_{bx}}{dy} \right)_{r_\alpha, r_\beta} \phi_\beta \right. \\ &\quad \left. + \phi_\alpha \frac{d\phi_\beta}{dr_{Ax}} \left(\frac{dr_{Ax}}{dy} \right)_{r_\alpha, r_\beta} \right] \\ &= -J^{5/3} r_\alpha r_\beta \phi_\alpha \phi_\beta \left[\frac{A}{B} \frac{\mathcal{L}_\alpha}{r_{bx}} + \frac{b}{a} \frac{\mathcal{L}_\beta}{r_{Ax}} \right], \end{aligned} \tag{5.18}$$

where $\mathcal{L}_\gamma$ is the logarithmic derivative

$$\mathcal{L}_\gamma = \frac{\phi_\gamma'}{\phi_\gamma} .$$

The relative rapidity of y dependence is

$$\frac{1}{N} \left(\frac{\partial N}{\partial y} \right)_{r_\alpha, r_\beta} = -J^{2/3} r_\alpha r_\beta \left[\frac{A}{A+x} \frac{\mathcal{L}_\alpha}{r_{bx}} + \frac{b}{b+x} \frac{\mathcal{L}_\beta}{r_{Ax}} \right] . \tag{5.19}$$

The right-hand side of this equation depends upon mass ratios [J, $A/(A+x)$, and $b/(b+x)$] and the logarithmic derivatives which are closely related to the local momenta of the bound states, and are of the order of the Fermi momentum on the average. We therefore expect a strong dependence of the overlap kernel on the angle between $\vec{r}_\alpha$ and $\vec{r}_\beta$ for reactions in which J is large and the bound-state wave functions have many nodes.[42] Such reactions correspond to heavy-ion-induced processes on massive targets with small mass transfer. However, for reactions in which appreciable mass is transferred and the bound-state functions are smooth, we expect smooth angle dependence and consequently rapid falloff with L, so that only the low partial waves will be influenced by nonorthogonality corrections. If many partial waves contribute and if the low partial waves are unimportant (because of strong absorption), then nonorthogonality will have little effect on the cross section. For ^{16}O$(d, p)^{17}$O the bound-state functions are rather slowly varying and the square root of the Jacobian, which roughly determines the overall strength, is only $J^{1/2} = 2.60$. For the ^{28}Si$(^{16}$O, ^{12}C$)^{32}$S reaction the bound states have a few more nodes than in ^{16}O$(d, p)^{17}$O; however, $J^{1/2}$ is still only 4.96.

A much larger Jacobian is obtained if only one nucleon is transferred in a heavy-ion process, for example ^{91}Zr$(^{16}$O, ^{17}O$)^{90}$Zr, where $J^{1/2} = 54.97$. It is of interest to estimate the maximum possible effect of nonorthogonality for this reaction and compare with the (d, p) case. For this purpose we assume that the eigenvalues are again given by the empirical formula, Eq. (5.12):

$$\lambda_{Ln} = s t^L p^n , \tag{5.20}$$

except that s and p take different values because

for ^{91}Zr(^{16}O, ^{17}O)^{90}Zr the rate of decrease with L is slower than for ^{16}O$(d, p)^{17}$O. Using Eqs. (5.14) and (5.16) we can eliminate s and then use Eq. (5.15) to obtain an approximate formula for the norm of N_L.

$$\| N_L \| \simeq \left[J \frac{(1-t)^2}{1+t} (1-p) t^L \right]^{1/2}. \tag{5.21}$$

The value of t (between 0 and 1) that maximizes this norm for the important surface partial wave L_s is approximately

$$t_{\max} = 1 - \frac{2}{L_s + 2} \quad (L_s \gg 1). \tag{5.22}$$

For these important partial waves the maximum norm is

$$\| N_{L_s} \| \simeq \frac{J^{1/2}}{L_s+2} \left(1 - \frac{2}{L_s+2}\right)^{L_s/2} \simeq \frac{J^{1/2} e^{-1}}{L_s+2} \quad (L_s \gg 1), \tag{5.23}$$

where in Eq. (5.21) we have assumed $p \simeq \frac{1}{2}$, the same value as the ^{16}O$(d, p)^{17}$O case. For the reaction ^{91}Zr(^{16}O, ^{17}O)^{90}Zr with $L_s = 30$, Eq. (5.23) gives

$$\| N_{L_s} \| \simeq 0.59, \tag{5.24}$$

which is about 5 times larger than the norm for ^{16}O$(d, p)^{17}$O with $L = 6$ (using Eq. 5.12). Since the nonorthogonality effect in the (d, p) case was about 10–15% it is quite possible that large effects could occur in the ^{91}Zr(^{16}O, ^{17}O)^{90}Zr process. Equation (5.23) indicates that the largest effects would be at low incident lab energies, which give lower values of $L_s = kR$. We intend to perform this calculation and shall report the results in a later communication.

We are now in a position to explain the conclusions of Sec. III. The limited strength and rapid decrease with increasing L of the overlap kernel is responsible for the small nonorthogonality effects obtained in the ^{16}O$(d, d)^{16}$O, ^{16}O$(d, p)^{17}$O, ^{17}O$(p, p)^{17}$O, ^{28}Si(^{16}O, ^{16}O)^{28}Si, and ^{28}Si(^{16}O, ^{12}C)^{32}S reactions. The destructive interference between nonorthogonality and channel coupling effects for ^{16}O$(d, d)^{16}$O and ^{16}O$(d, p)^{17}$O can be understood from Eqs. (2.49) and (2.50) which show that the coupling term is proportional to $1 - N^\dagger \Lambda_{\alpha\beta}$, which is well approximated by $1 - N^\dagger N$ because N is small. Since $N^\dagger N$ is positive, we obtain destructive interference. For ^{17}O$(p, p)^{17}$O the nonorthogonality contribution was very small, but constructive. As pointed out in Ref. 38 for ^{17}O$(p, p)^{17}$O the nonorthogonality effects, as we have defined them, do not contribute until third order in $K_{\alpha\beta}$. This can be seen by examining Eqs. (2.20), (2.21), and (2.24b), and noticing that $ND_\alpha f_\alpha = 0$, where f_α is the zero-order solution. Hence the overlap kernel N first enters in the third-order amplitude which, as will be shown in Sec. VII, is smaller than the second-order amplitude. Finally, the conclusion that nonorthogonality effects become larger when channel-coupling effects are more important follows trivially from Eqs. (2.58) and (2.60) or from Eq. (2.53). These equations show that the nonorthogonality potentials are also proportional to the interaction kernel I which must necessarily be larger if channel-coupling effects are to be important.

VI. SURFACE APPROXIMATION FOR MULTISTEP AMPLITUDES

In preparation for the analysis of the higher-order effects of the I kernel, we now develop a useful approximate expression for the multistep transition amplitude. Because this approximation exploits the surface dominance that is typical of reactions which involve strong absorption, it is called the surface approximation (SA). The present derivation complements that given in our previous note[38] on the SA.

We begin by writing Eqs. (3.1) and (3.2) as integral equations (neglecting nonorthogonality)

$$\chi_L^\alpha = f_L^\alpha + G_L^\alpha I_L^{\beta\alpha} \chi_L^\beta, \tag{6.1}$$

$$\chi_L^\beta = G_L^\beta I_L^\beta \chi_L^\alpha, \tag{6.2}$$

where f_L^α is a regular homogeneous solution of Eq. (3.1). The partial-wave Green's functions $G_L^\gamma (\gamma = \alpha, \beta)$ of the differential operators in Eqs. (3.1) and (3.2) can be written in the explicit form

$$G_L^\gamma(r_\gamma, r'_\gamma) = f_L^\gamma(r_<) h_L^\gamma(r_>)/W_L^\gamma, \tag{6.3a}$$

$$W_L^\gamma = \frac{\hbar^2}{2\mu_\gamma} \left[f^\gamma(r) \frac{dh^\gamma}{dr}(r) - h^\gamma(r) \frac{df^\gamma}{dr}(r) \right], \tag{6.3b}$$

the Wronskians W_L^γ being independent of radius. In Eq. (6.3a) h_L^γ is a homogeneous solution of Eq. (3.1) or Eq. (3.2) that is purely outgoing asymptotically, and the standard conventions $r_<$ $\equiv \min(r_\gamma, r'_\gamma)$, $r_> \equiv \max(r_\gamma, r'_\gamma)$ apply. Integral expressions for the rearrangement and elastic amplitudes follow from Eqs. (3.24), (3.25), (6.1), (6.2), and (6.3):

$$T_L^{\alpha\alpha} = t_L^\alpha + (W_L^\alpha)^{-1} \langle f_L^{\alpha *} | I_L^{\beta\alpha} | \chi_L^\beta \rangle, \tag{6.4}$$

$$T_L^{\beta\alpha} = (W_L^\beta)^{-1} \langle f_L^{\beta *} | I_L^{\beta\alpha} | \chi_L^\alpha \rangle. \tag{6.5}$$

Here t_L^α is the elastic scattering amplitude that would be produced by the diagonal potential U_α in channel α. Iterative application of Eqs. (6.1) and (6.2) to Eqs. (6.4) and (6.5) generates the

following two series:

$$T_L^{\alpha\alpha} = t_L^{\alpha} + (W_L^{\alpha})^{-1}\langle f_L^{\alpha *} | I_L^{\beta\alpha} G_L^{\beta} I_L^{\beta\alpha} | f_L^{\alpha}\rangle + \cdots , \tag{6.6}$$

$$T_L^{\beta\alpha} = T_L^{\beta\alpha}(\mathrm{DW}) + (W_L^{\beta})^{-1}\langle f_L^{\beta *} | I_L^{\beta\alpha} G_L^{\alpha} I_L^{\beta\alpha} G_L^{\beta} I_L^{\beta\alpha} | f_L^{\alpha}\rangle + \cdots . \tag{6.7}$$

In Eq. (6.7), $T_L^{\beta\alpha}(\mathrm{DW})$ is the DWBA transition amplitude:

$$T_L^{\beta\alpha}(\mathrm{DW}) = (W_L^{\beta})^{-1}\langle f_L^{\beta *} | I_L^{\beta\alpha} | f_L^{\alpha}\rangle . \tag{6.8}$$

To simplify the higher-order terms in Eqs. (6.6) and (6.7), we now make separable approximations to the Green's functions. In our approximation we assume all processes are dominated by strong absorption and surface localization. For such reactions it is sufficient, in obtaining the multistep amplitude, to describe the propagation of the intermediate state only in the region near the nuclear surface. Since the Green's function governs this propagation we need only compute $G_L^{\gamma}(r_\gamma, r'_\gamma)$ accurately for $r_\gamma \simeq r'_\gamma \simeq R$ to obtain good, approximate transition amplitudes. Here R is the effective nuclear radius. Because the partial-wave Green's function is symmetric and continuous we have from Eq. (6.3a)

$$f_L^{\gamma}(r_\gamma) h_L^{\gamma}(r'_\gamma) \simeq f_L^{\gamma}(r'_\gamma) h_L^{\gamma}(r_\gamma)$$

for $r_\gamma \simeq r'_\gamma$. For strongly absorbing processes the mean free path of intermediate propagation, measured by $|\vec{r}_\gamma - \vec{r}'_\gamma|$, is small. Hence the transition amplitudes should be fairly accurately reproduced, especially for the important surface partial waves, if one of the two approximate expressions

$$(W_L^{\gamma})^{-1} f_L^{\gamma}(r_\gamma) h_L^{\gamma}(r'_\gamma) \text{ or } (W_L^{\gamma})^{-1} f_L^{\gamma}(r'_\gamma) h_L^{\gamma}(r_\gamma)$$

is used in place of G_L^{γ} in Eqs. (6.6) and (6.7). Fortunately, there is no need to decide which expression to choose, since both lead to exactly the same approximate DW series when inserted in Eqs. (6.6) and (6.7):

$$T_L^{\alpha\alpha} = t_L^{\alpha} + D_L^{\alpha\beta} T_L^{\beta\alpha}(\mathrm{DW}) + D_L^{\alpha\beta} D_L^{\beta\alpha} T_L^{\beta\alpha}(\mathrm{DW}) + \cdots , \tag{6.9}$$

$$T_L^{\beta\alpha} = T_L^{\beta\alpha}(\mathrm{DW}) + D_L^{\beta\alpha} D_L^{\alpha\beta} T_L^{\beta\alpha}(\mathrm{DW}) + \cdots , \tag{6.10}$$

where

$$D_L^{\beta\alpha} \equiv (W_L^{\beta})^{-1}\langle f_L^{\beta *} | I_L^{\beta\alpha} | h_L^{\alpha}\rangle , \tag{6.11}$$

$$D_L^{\alpha\beta} \equiv (W_L^{\alpha})^{-1}\langle f_L^{\alpha *} | I_L^{\beta\alpha} | h_L^{\beta}\rangle . \tag{6.12}$$

Each of the two series can now be summed to give the closed-form results

$$T_L^{\alpha\alpha} = t_L^{\alpha} + D_L^{\alpha\beta} T_L^{\beta\alpha}(\mathrm{DW})(1 - D_L^{\alpha\beta} D_L^{\beta\alpha})^{-1}, \tag{6.13}$$

$$T_L^{\beta\alpha} = T_L^{\beta\alpha}(\mathrm{DW})(1 - D_L^{\beta\alpha} D_L^{\alpha\beta})^{-1}. \tag{6.14}$$

It is interesting that Eq. (6.14) has the form of a renormalized DWBA amplitude. These results differ from those given in Ref. 38, because in that work a different method if iteration was used in place of Eqs. (6.6) and (6.7).

Our separable approximation for the Green's function $f_L^{\gamma}(r_\gamma) h_L^{\gamma}(r'_\gamma)$ or $f_L^{\gamma}(r'_\gamma) h_L^{\gamma}(r_\gamma)$, is not the best possible approximation because of the presence of the function h_L^{γ}, which becomes infinite at the origin. This would force the result of our separable approximation acting on any function also to be infinite at the origin. We know, however, that the Green's function terms in Eqs. (6.1) and (6.2) are regular at the origin, though they are asymptotically outgoing. The difference between two regular scattering solutions corresponding to two different potentials is guaranteed to have both of these desirable properties. We therefore replace h_L^{γ} by the function $\bar{h}_L^{\gamma}$ given by

$$\bar{h}_L^{\gamma}(r_\gamma) = c_L^{\gamma}(\tilde{f}_L^{\gamma}(r_\gamma) - f_L^{\gamma}(r_\gamma)),$$

where the regular function $\tilde{f}_L^{\gamma}$ is a scattering solution corresponding to a different distorting potential. The constant c_L^{γ} is to be chosen so that $\bar{h}_L^{\gamma} \to h_L^{\gamma}$ for large r_γ. Since, asymptotically,

$$f_L^{\gamma} \to F_L^{\gamma} + t_L^{\gamma} H_L^{\gamma},$$

$$\tilde{f}_L^{\gamma} \to F_L^{\gamma} + \tilde{t}_L^{\gamma} H_L^{\gamma},$$

$$h_L^{\gamma} \to H_L^{\gamma},$$

we find

$$c_L^{\gamma} = (\tilde{t}_L - t_L^{\gamma})^{-1}. \tag{6.15}$$

This gives

$$\bar{h}_L^{\gamma} = (\tilde{t}_L^{\gamma} - t_L^{\gamma})^{-1}(\tilde{f}_L^{\gamma} - f_L^{\gamma}), \tag{6.16}$$

which has the correct behavior for large r_γ. Here $\tilde{t}_L^{\gamma}$ is the elastic scattering amplitude calculated for an optical potential obtained by adding an auxiliary potential to the diagonal interaction U_γ.

Combining Eqs. (6.11), (6.12), and (6.16) gives the final result for the surface approximation (SA):

$$D_L^{\beta\alpha} = (W_L^{\beta})^{-1}\langle f_L^{\beta *} | I_L^{\beta\alpha} | \bar{h}_L^{\alpha}\rangle = \frac{\tilde{T}_L^{\beta\alpha}(\mathrm{DW}) - T_L^{\beta\alpha}(\mathrm{DW})}{\tilde{t}_L^{\alpha} - t_L^{\alpha}} , \tag{6.17}$$

$$D_L^{\alpha\beta} = (W_L^{\alpha})^{-1}\langle f_L^{\alpha *} | I_L^{\beta\alpha} | \bar{h}_L^{\beta}\rangle = \frac{\tilde{T}_L^{\alpha\beta}(\mathrm{DW}) - T_L^{\alpha\beta}(\mathrm{DW})}{\tilde{t}_L^{\beta} - t_L^{\beta}} . \tag{6.18}$$

The transition amplitudes $\tilde{T}_L^{\beta\alpha}(\mathrm{DW})$ and $\tilde{T}_L^{\alpha\beta}(\mathrm{DW})$ are DWBA amplitudes using the auxiliary distorted

waves $\tilde{f}_L^{\alpha}$ and $\tilde{f}_L^{\beta}$, respectively, in the right-hand side of the matrix element. The SA amplitudes defined by Eqs. (6.13), (6.14), (6.17), and (6.18) can all be calculated by using standard DWBA codes. As shown in Ref. 38, a surface-peaked form should be used for the auxiliary potential that is added to U_γ to generate the quantities $\tilde{T}_L^{\beta\alpha}(\mathrm{DW})$, $\tilde{T}_L^{\alpha\beta}(\mathrm{DW})$, $\tilde{t}_L^{\alpha}$, and $\tilde{t}_L^{\beta}$. The motivation for this choice, and the importance of using a realistic diffuseness for the auxiliary potential, are discussed in that work.

Although our approximate representation of the Green's function is not symmetric under interchange of r_γ and r'_γ, our final results, Eqs. (6.13), (6.14), (6.17), and (6.18), possess the symmetry implied by time-reversal invariance. A different separable approximation to the Green's function, symmetric in r_γ and r'_γ, is the well-known on-shell approximation (OS)[32,43,44]:

$$G_L^{\gamma}(r_\gamma, r'_\gamma) \to i \frac{f_L^{\gamma}(r_\gamma) f_L(r'_\gamma)}{W_L^{\gamma} S_L^{\gamma}} .$$

The quantity S_L^{γ} is the elastic S matrix for channel γ. The OS gives the same closed-form expressions for the transition amplitudes, Eqs. (6.13) and (6.14), but now Eqs. (6.17) and (6.18) become (for OS)

$$D_L^{\beta\alpha} = i \frac{\langle f_L^{\beta *} | I_L^{\beta\alpha} | f_L^{\alpha} \rangle}{W_L^{\alpha} S_L^{\alpha}} = \frac{i T_L^{\beta\alpha}(\mathrm{DW})}{S_L^{\alpha}}, \tag{6.19}$$

$$D_L^{\alpha\beta} = i \frac{\langle f_L^{\alpha *} | I_L^{\beta\alpha} | f_L^{\beta} \rangle}{W_L^{\beta} S_L^{\beta}} = i \frac{T_L^{\alpha\beta}(\mathrm{DW})}{S_L^{\beta}} . \tag{6.20}$$

The OS also preserves time-reversal invariance; however, it does not have as clear a physical interpretation as the SA, and gives less accurate results for strong-absoprtion processes. In the numerical applications of the OS, presented in the next section, we find that for the important surface partial waves the multistep contributions are overestimated. This is because strong absorption is still present in the elastic channel for these partial waves and the magnitude of S_L^{γ}, which is in the denominator of Eqs. (6.19) and (6.20), is about 0.2. This conclusion, that the OS tends to overestimate the multistep amplitudes, was also reached by Robson[32] from a different point of view.

VII. INTERPRETATION OF CHANNEL-COUPLING EFFECTS

In this section we complete our discussion of higher-order phenomena by analyzing the channel-coupling effects produced by the I kernel alone. The results that are summarized in Sec. IV lead us to ask first: why are the channel-coupling effects important for light-ion-induced reactions but not for heavy-ion processes? We would also like to understand why these effects are larger for elastic scattering than for rearrangement, and why the $^{17}O(p,p)^{17}O$ reaction shows a larger percentage effect than the $^{16}O(d,d)^{16}O$ reaction. Finally, we wish to explain why the behavior of the channel-coupling effects is so systematically similar to the behavior of the rearrangement amplitude, when the model parameters are varied.

To answer these questions we apply the SA and, for comparison, the OS to the elastic reactions $^{17}O(p,p)^{17}O$, $^{16}O(d,d)^{16}O$, $^{28}Si(^{16}O, ^{16}O)^{28}Si$, and $^{32}S(^{12}C, ^{12}C)^{32}S$ for which exact coupled-channels calculations were reported in Sec. IV. Using Eqs. (6.13), (6.14), (6.17), (6.18), (6.19), and (6.20) along with the same model parameters given in Sec. IV, we have obtained approximate amplitudes and cross sections. The results are displayed in Figs. 12–16, where comparison is made between exact higher-order calculations and the predictions of the SA and OS. Because the higher-order effects were so small for the two heavy-ion cases, the calculations were carried out only through second order in the I kernel. Furthermore, to make the effects more readily visible, we have artificially enhanced them tenfold by increasing the product of spectroscopic amplitudes, Eq. (4.1), which enters exact, SA, and OS calculations. Figure 14 is a comparison between lowest-order and second-order calculations for $^{32}S(^{12}C, ^{12}C)^{32}S$ elastic scattering and indicates the (unrealistic) size of the higher-order effect which the SA and OS are trying to approximate. The predictions of the SA and OS are shown in Figs. 15 and 16.

It is apparent from Figs. 13, 15, and 16 that the SA is a very good approximation for the multistep amplitude when strong absorption is present.

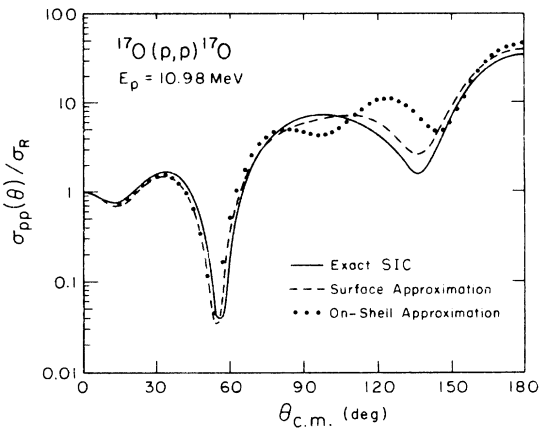

FIG. 12. Comparison of exact SIC with the SA and OS for $^{17}O(p,d,p)^{17}O$.

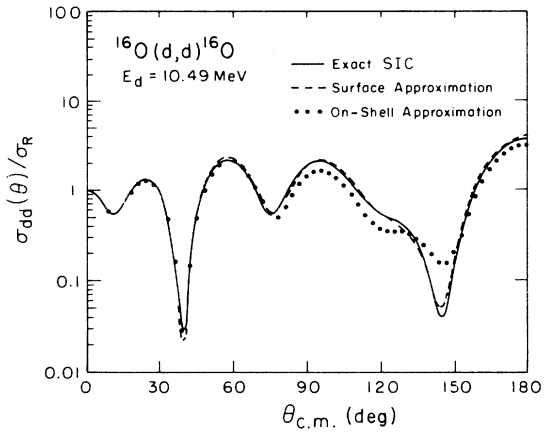

FIG. 13. Comparison of exact SIC with the SA and OS for $^{16}O(d,p,d)^{16}O$.

Even for $^{17}O(p,p)^{17}O$, which does not involve strongly absorbed particles in the initial and final states, the SA predictions are quite reasonable. The on-shell approximation does not do well, especially for the heavy-ion reactions, and tends to overestimate the multistep contribution. It appears that the OS may only be useful in a qualitative fashion in contrast to the quantitative success of the SA.

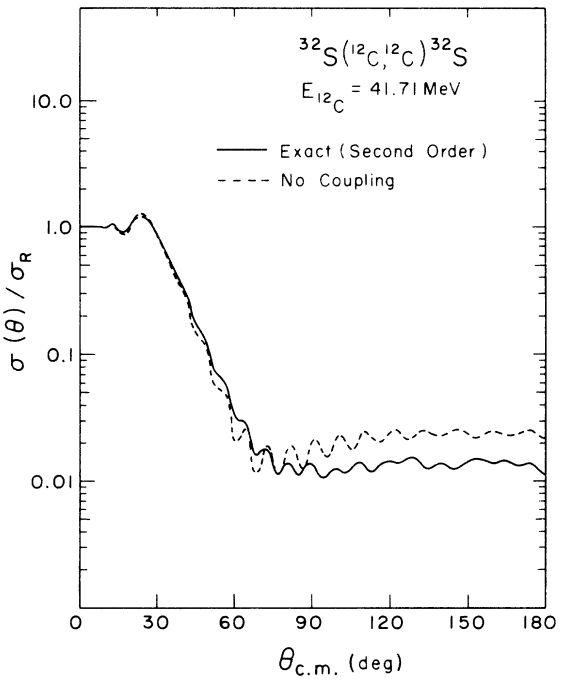

FIG. 14. Comparison of the exact second-order SIC calculation with the lowest-order no-coupling result for $^{32}S(^{12}C,^{12}C)^{32}S$. The size of the effect has been enhanced by an unrealistic increase in the coupling strength.

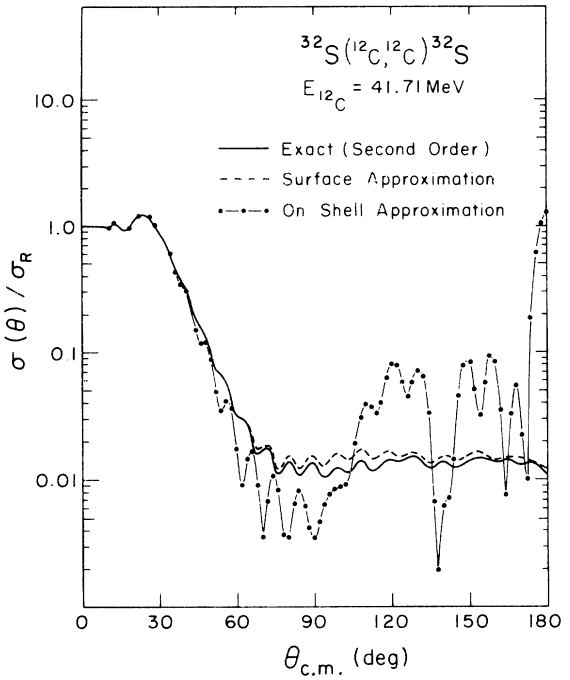

FIG. 15. Comparison of exact second-order SIC calculation with the SA and OS for $^{32}S(^{12}C,^{16}O,^{12}C)^{32}S$.

Because the OS overestimates the multistep amplitudes, we use this approximation to explain, in a qualitative fashion, the relative size of the channel-coupling effects for light-ion and heavy-ion reactions. For simplicity consider second order, in which the multistep amplitudes is proportional to one D_L amplitude for elastic scattering,

$$T_L^{\alpha\alpha} = D_L^{\alpha\beta}\, T_L^{\beta\alpha}(\mathrm{DW}) \quad (\text{2nd order}), \tag{7.1}$$

and two for rearrangement,

$$T_L^{\beta\alpha} = D_L^{\beta\alpha} D_L^{\alpha\beta}\, T_L^{\beta\alpha}(\mathrm{DW}) \quad (\text{2nd order}). \tag{7.2}$$

Since $D_L^{\beta\alpha} = iT_L^{\beta\alpha}(\mathrm{DW})/S_L^{\alpha}$ in the on-shell approximation, the relative size of the effect is characterized by the ratio of a rearrangement amplitude to an elastic S matrix. For the important (i.e., surface) partial waves the magnitude of S_L varies from 0.2 to 0.5 for both light-ion and heavy-ion scattering, while the magnitude of the rearrangement amplitude is much smaller, typically 0.1 for light ions and 0.01 for heavy ions. Consequently channel-coupling effects are expected to be much more important for light-ion-induced reactions (where $|D_L| \simeq \frac{1}{5}$ to $\frac{1}{2}$) than for heavy-ion-induced processes (where $|D_L| \simeq \frac{1}{50}$ to $\frac{1}{20}$). This agrees with our detailed calculations and explains why only small effects are obtained in the heavy-ion calculations. Physically, the effects are small because elastic scattering is much more probable

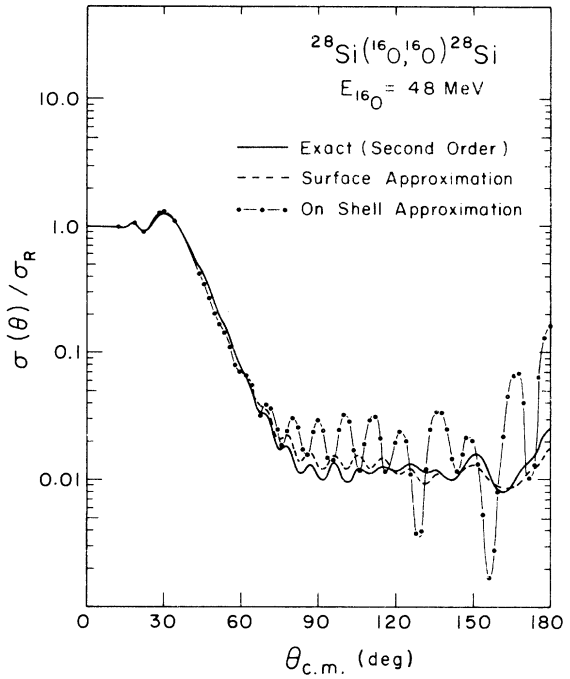

FIG. 16. Comparison of exact second-order SIC calculation with the SA and OS for ^{28}Si(^{16}O, ^{12}C, ^{16}O)^{28}Si.

than rearrangement for heavy-ion processes. Since the magnitude of D_L is less than unity we see that third-order effects are smaller than second-order and that, for our applications, multistep contributions are more important for elastic than for rearrangement scattering.

To explain why the ^{17}O(p, p)^{17}O reaction showed a larger percentage channel-coupling effect than the ^{16}O(d, d)^{16}O reaction we compare, in second order, the relative effect Δ predicted by the OS. For ^{17}O(p, p)^{17}O we have

$$\Delta_{pp} = \frac{|D_L^{pd}|\,|T_L^{dp}(\mathrm{DW})|}{|T_L^{pp}|} = \frac{|T_L^{pd}(\mathrm{DW})|\,|T_L^{dp}(\mathrm{DW})|}{|T_L^{pp}|\,|S_L^{d}|} \tag{7.3}$$

while for ^{16}O(d, d)^{16}O

$$\Delta_{dd} = \frac{|D_L^{dp}|\,|T_L^{pd}(\mathrm{DW})|}{|T_L^{dd}|} = \frac{|T_L^{dp}(\mathrm{DW})|\,|T_L^{pd}(\mathrm{DW})|}{|T_L^{dd}|\,|S_L^{p}|}\,. \tag{7.4}$$

Equations (7.3) and (7.4) make clear why the percentage effect is larger for proton elastic scattering. The numerators in these two equations are identical, but the denominator for proton elastic scattering, Eq. (7.3), is somewhat smaller. This is because the deuteron is more strongly absorbed, $|S_L^d| < |S_L^p|$ for surface partial waves, and because the proton elastic amplitude is not as large as the deuteron amplitude, $|T_L^{pp}| < |T_L^{dd}|$.

The last phenomenon to be explained is the strong correlation between channel-coupling effects and the rearrangement amplitude. This result follows trivially from both the SA and the OS since in both approximations the higher-order amplitudes are approximately quadratic or cubic functions of the DWBA rearrangement amplitudes. Another consequence is that the L dependence of the multistep amplitude can be inferred from the L dependence of the DWBA rearrangement amplitude. Because the DWBA rearrangement amplitude is localized in L space around the surface partial waves, the higher-order amplitude is also localized, and the important contributions from multistep processes occur predominantly at the nuclear surface. Moreover, since the rearrangement amplitude tends to fall off more slowly with L than the elastic amplitude does, the multistep contributions to elastic scatterings are of longer range than the folded distorting potentials.

VIII. SUMMARY AND CONCLUSIONS

One of the major results of this work is that channel nonorthogonality effects can be understood in terms of a single geometric object, the overlap kernel N. By studying this quantity we have been able to explain why the nonorthogonality effects were found to be small both for the light-ion- and heavy-ion-induced reactions considered in this paper. As shown in Sec. V, the effect is small because N_L decreases rapidly with L. Consequently the important (surface) partial waves are influenced very little. Our theoretical analysis of the overlap kernel leads us to suggest that nonorthogonality effects may be more important for processes in which a small mass is transferred from a low-momentum, heavy projectile to a heavy target. The reaction ^{91}Zr(^{16}O, ^{17}O)^{90}Zr at low lab energies would be a good candidate. Because our applications only included two arrangements, it is not clear if nonorthogonality effects will be large for the general case involving many arrangements. It is possible, however, that increasing the size of the model space may enhance the importance of the nonorthogonality corrections. Further study appears necessary on this point.

The channel-coupling effects from the interaction kernel I are found to be larger than nonorthogonality effects, especially for the light-ion-induced reactions. Using the surface and on-shell approximations we are able to understand the size and mechanism of the multistep processes.

Although the OS systematically overestimates the important partial-wave transition amplitudes, it provides qualitative insight into the higher-order effects. The SA is much more successful in quantitatively reproducing the channel-coupling effects. Both the SA and OS expressions depend explicitly on the DWBA rearrangement amplitudes. From this we conclude that the multistep processes are predominantly surface localized (whenever this is true of DWBA) and that channel-coupling effects are long ranged. Furthermore, the fact that the S-matrix element for rearrangement is much smaller than that for elastic scattering in the heavy-ion applications allows us to explain why the higher-order coupling effects are small for these reactions. The effects of a single intermediate channel are very small for the heavy-ion processes. Probably the most important way of improving the higher-order treatment of these reactions would be to include a large number of different arrangements and channels.

Finally, the smallness of nonorthogonality effects suggests that there is often no practical difference between the MS method and the method based on the UIC equations, proposed by Kunz, or the more convenient SIC equations of Sec. II. We therefore conclude that reactions for which nonorthogonality is not important may be analyzed using any of the three approaches, since the three formulations differ only by terms proportional to N.

ACKNOWLEDGMENTS

The authors are grateful to N. Austern for many helpful clarifying discussions, and in particular for his emphasis on the consistency of the model-space method. R. M. Drisko and F. Tabakin gave timely and much appreciated advice.

APPENDIX: LINEAR INDEPENDENCE AND PROPERTIES OF THE OVERLAP KERNEL

First, we investigate the linear independence of the set of vectors

$$B \equiv \{ \Phi_{\gamma \vec{r}}, \quad \gamma = \alpha, \beta, \text{ all } \vec{r} \}, \tag{A1}$$

which spans the model space $\mathcal{L}_M$ that was introduced in Sec. II. Though it is usually disregarded, this question is of direct practical significance. Linear dependence of the set B would imply that the corresponding coefficients, namely $\chi_\gamma(\vec{r})$ $(\gamma = \alpha, \beta)$ in Eq. (2.16), are not uniquely determined, even when the wave function $\Psi_M \epsilon \mathcal{L}_M$ is known. More specifically, linear dependence of B would imply existence of nonzero functions ζ_γ $(\gamma = \alpha, \beta)$ such that

$$\int d\vec{r} \sum_{\gamma=\alpha,\beta} \zeta_\gamma(\vec{r}) \Phi_{\gamma \vec{r}} = 0. \tag{A2}$$

Consequently, $\chi_\gamma(\vec{r})$ would be indeterminate up to an arbitrary multiple of ζ_γ.

Forming the scalar product of Eq. (A2) with $\Phi_{\gamma' \vec{r}'}$ gives the result

$$\int d\vec{r} \sum_{\gamma=\alpha,\beta} \langle \Phi_{\gamma' \vec{r}'} | \Phi_{\gamma \vec{r}} \rangle \zeta_\gamma(\vec{r}) = 0. \tag{A3}$$

We now introduce the *overlap kernels* defined by

$$w_{\gamma'\gamma}(\vec{r}', \vec{r}) \equiv \langle \Phi_{\gamma' \vec{r}'} | \Phi_{\gamma \vec{r}} \rangle,$$

which can conveniently be grouped to form a matrix of kernels:

$$\underline{w} \equiv \begin{pmatrix} w_{\alpha\alpha}(\vec{r}', \vec{r}) & w_{\alpha\beta}(\vec{r}', \vec{r}) \\ w_{\beta\alpha}(\vec{r}', \vec{r}) & w_{\beta\beta}(\vec{r}', \vec{r}) \end{pmatrix}. \tag{A4}$$

Analogously regarding $\zeta_\alpha(\vec{r})$ and $\zeta_\beta(\vec{r})$ as a column matrix $\underline{\zeta}$, we can write Eq. (A3) in the form

$$\underline{w}\,\underline{\zeta} = 0. \tag{A5}$$

If B is linearly dependent, Eq. (A5) has a nonzero solution $\underline{\zeta}$, so that $\underline{w}$ has zero as an eigenvalue. Equivalently, if zero is *not* an eigenvalue of $\underline{w}$, then B is linearly *in*dependent. This suggests our strategy for proving linear independence: we simily compute eigenvalues of $\underline{w}$.

The eigenvalue problem for the matrix $\underline{w}$ can be reduced to an eigenvalue problem for a single symmetric kernel. We write

$$\underline{w} = \begin{pmatrix} \delta(\vec{r}' - \vec{r}) & N(\vec{r}', \vec{r}) \\ N^*(\vec{r}, \vec{r}') & \delta(\vec{r}' - \vec{r}) \end{pmatrix} = \begin{pmatrix} 1 & N \\ N^\dagger & 1 \end{pmatrix} \tag{A6}$$

using a notation introduced in Sec. II,

$$N(\vec{r}', \vec{r}) \equiv \langle \Phi_{\alpha \vec{r}'} | \Phi_{\beta \vec{r}} \rangle = w_{\alpha\beta}(\vec{r}', \vec{r}), \tag{A7}$$

and the easily derived relations

$$w_{\alpha\alpha}(\vec{r}', \vec{r}) = w_{\beta\beta}(\vec{r}', \vec{r}) = \delta(\vec{r}' - \vec{r}), \tag{A8}$$

$$w^*_{\alpha\beta}(\vec{r}', \vec{r}) = w_{\beta\alpha}(\vec{r}, \vec{r}'). \tag{A9}$$

If the trivial unit-diagonal part of $\underline{w}$ in Eq. (A6) is removed, the remaining matrix

$$\underline{\mathfrak{N}} \equiv \begin{pmatrix} 0 & N \\ N^\dagger & 0 \end{pmatrix} \tag{A10}$$

still contains complete information about the kinematic effects of nonorthogonality. Consider the square of this matrix, explicitly given by

$$(\underline{\mathfrak{N}})^2 = \begin{pmatrix} NN^\dagger & 0 \\ 0 & N^\dagger N \end{pmatrix}. \tag{A11}$$

From Eqs. (A6) and (A11), the eigenvalues of

w are clearly related to those of

$$\eta = NN^{\dagger} \tag{A12a}$$

and

$$\tilde{\eta} = N^{\dagger}N. \tag{A12b}$$

Note that η and $\tilde{\eta}$ have the same eigenvalues.

Because $\underline{\mathfrak{N}}$ is Hermitian, its Hilbert-Schmidt (HS) norm is

$$\|\underline{\mathfrak{N}}\|_{\mathrm{HS}} \equiv [\mathrm{tr}(\underline{\mathfrak{N}}^2)]^{1/2} = (2\,\mathrm{tr}\eta)^{1/2} \tag{A13}$$

by Eqs. (A11) and (A12). By calculation that is mentioned in Sec. V, this trace is equal to a Jacobian [Eq. (2.15)], which is determined solely by mass ratios:

$$\mathrm{tr}\eta = J = \left[\frac{a(A+x)}{x(A+a)}\right]^3. \tag{A14}$$

By a well-known theorem,[46] the finiteness of (A13) implies that $\mathfrak{N}$ is a compact operator, so that its spectrum is bounded and discrete, with zero as the only possible point of accumulation. The same must be true of $\mathfrak{N}^2$ and therefore, by Eq. (A11), also of η. Let the eigenvalues of η (in order of decreasing magnitude) be

$$\lambda_0 \geq \lambda_1 \geq \lambda_2 \cdots \geq 0. \tag{A15}$$

These eigenvalues are nonnegative because every expectation of η is nonnegative. Corresponding to each eigenvalue λ_m of η, the overlap matrix $\underline{w}$ has a pair of eigenvalues

$$w_m^{(\pm)} = 1 \pm (\lambda_m)^{1/2}. \tag{A16}$$

Therefore, provided that none of the λ_m is unity, i.e., provided that

$$\lambda_m \neq 1 \quad (m = 0, 1, 2\ldots), \tag{A17}$$

$\underline{w}$ does *not* have a zero eigenvalue, and the Set $\overline{B}$ is linearly *in*dependent.

Together with the spectral properties of η, Eq. (A16) shows that $\underline{w}$ has only discrete eigenvalues of finite degeneracy, and that their only point of accumulation is 1. If, by accident, some eigenvalue of $\underline{w}$ were exactly zero, the Set B would be linearly dependent, but a small adjustment of the bound-state parameters would restore linear independence. Thus, for practical purposes linear independence is assured.

Once the set of vectors B is known to be linearly independent, it is reasonable to ask if the solution of the coupled integro-differential equations (Sec. II) is unique. The equations can be written as integral equations of Lippmann-Schwinger type by applying the Green's functions of the differential operators D_γ. If the energy has a positive imaginary part $i\epsilon$, the resulting equations are of Fredholm form provided that the interactions are bounded, as we assume. Consequently, their solution is unique. Also, Coester[47] has described a method of rewriting such equations in a form such that the kernel has a finite HS norm even in the physical limit $\epsilon \to 0+$. Thus the solution of the coupled equations (subject to the appropriate boundary conditions) is unique.

For the particular case of the coupled d and p channels with an ^{16}O core, we have numerically investigated the spectrum of $\underline{w}$. Because the bound states are s wave, $\underline{w}$ and η do not connect different relative angular momenta L. Therefore, the eigenvalues λ_m and eigenvectors f_m may be characterized by two labels L, n in place of the single index m. This symmetry property is easily exploited by expressing η in terms of partial-wave kernels η_L. The compactness of η (and hence η_L) ensures that η_L can be uniformly approximated by simply replacing the implied integrations by finite summations. As a result, numerical diagonalization of fairly small finite matrices gives good approximations to the largest few eigenvalues of η. These eigenvalues are found to be quite accurately summarized by the simple formula

$$\lambda_{Ln} = s t^L p^n \tag{A18a}$$

with parameters

$$s = 0.37, \quad t = 0.59, \quad p = 0.45. \tag{A18b}$$

No explanation has been found for this surprisingly pure exponential dependence. We note that the sum rule (A14) provides a check on the formula (A18). We find

$$J = \sum_{n=0}^{\infty}\sum_{L=0}^{\infty} \lambda_{Ln} = \sum_{n=0}^{\infty}\sum_{L=0}^{\infty} (2L+1) s t^L p^n$$

$$\simeq \frac{s(1+t)}{(1-p)(1-t)^2} = 6.36,$$

in quite good agreement with the value implied by Eq. (A14):

$$J = \left[\frac{2.17}{1.18}\right]^3 = 6.74.$$

From the fact that the largest eigenvalue of η is $\lambda_{00} = 0.37$, we can use Eq. (A16) to conclude that the smallest eigenvalue of $\underline{w}$ is 0.39. Consequently, for this case there is no danger of linear dependence.

Those eigenfunctions of η that correspond to the maximum eigenvalues (λ_{L0}) all show broad surface peaks without oscillations. Those that correspond to the smaller eigenvalues $\lambda_{Ln}\,(n > 0)$ have more nodes as n increases. Therefore the smaller eigenvalues may have some importance for reactions in which high momenta play a role.

We conclude by briefly remarking on some other mathematical consequences of the smallness of λ_{00}. First, the inverse of $\underline{w}$ finds application in some of the formulations of the MS method discussed in Sec. II. Its evaluation can be reduced to inversion of $(1-\eta)$. If $\lambda_{00} \ll 1$, the expansion

$$(1-\eta)^{-1} = 1 + \eta + \eta^2 + \cdots , \tag{A19}$$

converges rapidly, and may provide a useful algorithm. Since different partial waves are independent, one may consider η_L, the η operator for a given L. Then rapid convergence of the series for $(1-\eta_L)^{-1}$ requires only the (generally less restrictive) condition $\lambda_{L0} \ll 1$.

Generally, the size of any operator A is conveniently measured by its uniform norm $\|A\|$, defined as the square root of the largest eigenvalue of $A^{\dagger}A$. In particular,

$$\|(1-\eta_L)^{-1}\| = \max_m \{|1-\lambda_{Lm}|^{-1}\}. \tag{A20}$$

Consequently, if η_L has an eigenvalue near 1, $(1-\eta_L)^{-1}$ is a large operator. This remark is relevant to the discussion of the coupled equations (Sec. V). The following mathematical result is tacitly assumed and repeatedly applied: the norm of the product AB is bounded by $\|A\| \cdot \|B\|$, i.e.,

$$\|AB\| \leq \|A\| \cdot \|B\|. \tag{A21}$$

Hence if $\|\eta_L\|$ is small, $\|(1-\eta_L)^{-1}\|$ will be nearly 1 and so operators involving products of η_L and $(1-\eta_L)^{-1}$ will be small.

Finally, we note that the operator $\underline{w}^{-1/2}$ can be expanded in the form

$$\underline{w}^{-1/2} = \underline{1} - \tfrac{1}{2}\underline{\mathfrak{N}} + \tfrac{3}{8}(\underline{\mathfrak{N}})^2 - \cdots ,$$

which also converges rapidly if $\lambda_{00} \ll 1$. This operator can be used to construct an orthonormalized basis

$$\Phi^{ON}_{\gamma\vec{r}} \equiv \sum_{\gamma'=\alpha,\beta} \int d\vec{r}\,' \langle \gamma\vec{r}|\underline{w}^{-1/2}|\gamma'\vec{r}\,'\rangle \Phi_{\gamma'\vec{r}\,'}, \qquad (\gamma = \alpha, \beta), \tag{A22}$$

which spans the same model space $\mathcal{L}_M$ as the Set B.

---

*Supported in part by the National Science Foundation.

[1]W. Tobocman, Phys. Rev. 115, 98 (1959); 94, 1655 (1964); *Theory of Direct Nuclear Reactions* (Oxford U. P., London, 1961).

[2]R. H. Bassel, R. M. Drisko, and G. R. Satchler, Oak Ridge Report No. 3240, 1962 (unpublished).

[3]N. Austern, in *Fast Neutron Physics*, edited by J. B. Marion and J. L. Fowler (Interscience, New York, 1963), Vol. II.

[4]N. Austern, R. M. Drisko, E. C. Halbert, and G. R. Satchler, Phys. Rev. 133, B3 (1964).

[5]G. R. Satchler, *Lectures in Theoretical Physics* (Univ. of Colorado Press, Boulder, 1966), Vol. 8, p. 72.

[6]F. Pougheon *et al.*, Phys. Rev. Lett. 34, 158 (1975).

[7]F. Yagi *et al.*, Phys. Rev. Lett. 34, 96 (1972).

[8]R. J. Ascuitto *et al.*, Nucl. Phys. A226, 454 (1974).

[9]D. K. Kovar *et al.*, Phys. Rev. Lett. 33, 1611 (1974).

[10]U. Götz *et al.*, Phys. Rep. 16C, 115 (1975).

[11]S. K. Penny and G. R. Satchler, Nucl. Phys. 53, 145 (1964).

[12]P. J. Iano and N. Austern, Phys. Rev. 151, 853 (1966).

[13]P. D. Kunz, E. Rost, and R. R. Johnson, Phys. Rev. 177, 720 (1968).

[14]R. J. Ascuitto and N. K. Glendenning, Phys. Rev. 181, 1396 (1969).

[15]T. Tamura and T. Udagawa, Phys. Rev. C 5, 1127 (1972).

[16]P. Bindal and R. Koshel, Phys. Rev. C 6, 2281 (1972).

[17]A. P. Stamp, Nucl. Phys. 83, 232 (1966).

[18]G. R. Rawitscher, Phys. Rev. 163, 1223 (1967).

[19]N. Austern, Phys. Rev. 188, 1595 (1969).

[20]R. J. Ascuitto, N. K. Glendenning, and B. Sorensen, Nucl. Phys. A170, 65 (1970).

[21]R. Schaeffer and G. Bertsch, Phys. Lett. 38B, 159 (1972).

[22]L. J. B. Goldfarb and K. Takeuchi, Nucl. Phys. A181, 609 (1972).

[23]W. R. Coker, T. Udagawa, and H. H. Wolter, Phys. Lett. 41B, 237 (1972); Phys. Rev. C 7, 1154 (1973).

[24]T. Udagawa, H. H. Wolter, and W. R. Coker, Phys. Rev. Lett. 31, 1507 (1973).

[25]P. D. Kunz and E. Rost, Phys. Lett. 47B, 136 (1973).

[26]N. B. De Takacsy, Phys. Rev. Lett. 31, 1007 (1973); Phys. Lett. 42B, 1 (1973).

[27]R. A. Broglia, U. Götz, M. Ichimura, T. Kammuri, and A. Winther, Phys. Lett. 45B, 23 (1973).

[28]B. Imanishi, M. Ichimura, and M. Kawai, Phys. Lett. 52B, 267 (1974).

[29]S. R. Cotanch, Phys. Lett. 57B, 123 (1975).

[30]L. D. Faddeev, Zh. Eksp. Teor. Fiz. 39, 1459 (1960) [Sov. Phys.–JETP 12, 1014 (1961)].

[31]P. D. Kunz (private communication).

[32]D. Robson, Phys. Rev. C 7, 1 (1973).

[33]M. Baer and D. J. Kouri, J. Math. Phys. 14, 1637 (1973).

[34]E. F. Redish, Phys. Rev. C 10, 67 (1974).

[35]W. Tobocman, Phys. Rev. C 11, 352 (1975).

[36]D. J. Kouri and F. S. Levin, Phys. Rev. C 11, 352 (1975).

[37]T. Ohmura, B. Imanishi, M. Ichimura, and M. Kawai, Prog. Theor. Phys. 41, 391 (1969); 43, 347 (1970); 44, 1242 (1970).

[38]S. R. Cotanch and C. M. Vincent, Phys. Rev. Lett. 36, 21 (1976).

[39]We suppress complex conjugate notation since the bound-state functions may be taken real for s-wave relative motion.

[40]J. C. Peng and J. V. Maher (private communication).

[41]R. M. DeVries, G. R. Satchler, and J. G. Kramer, Phys. Rev. Lett. 32, 1377 (1974).

[42]Another geometry that gives rapid angle dependence and slow falloff with increasing L arises when the colliding fragments have very different radii.
[43]N. Austern, R. M. Drisko, E. Rost, and G. R. Satchler, Phys. Rev. 128, 733 (1962).
[44]P. Bindal and R. Koshel, Phys. Rev. C 6, 2281 (1972).
[45]D. Wilmore and P. E. Hodgson, Nucl. Phys. 55, 673 (1964).
[46]R. G. Newton, *Scattering Theory of Waves and Particles* (McGraw-Hill, New York, 1966), pp. 201, 202.
[47]F. Coester, Phys. Rev. 133, B1516 (1964).